Australian Government
Department of Defence
Science and Technology

Target Plate Deformation Time-History from a Detonating Buried Charge in Various Sand Media

S. A. Weckert and A. D. Resnyansky

Weapons and Combat Systems Division
Defence Science and Technology Group

DST-Group-TR-3609

ABSTRACT

The present work analysed the influence of the sand/soil media for deforming a target plate in response to loading from a buried explosive charge. Flash x-ray technique was used to capture the plate deformation as a measure of the momentum transfer to the target. The target response was assessed experimentally for a variety of sands and a soil to investigate the effect of the sand parameters. The experiments used an axisymmetric cylindrical setup to enable easier comparison with numerical simulations in two-dimensions. The experiments were used to validate a two-phase model for the sand which has been implemented in the CTH hydrocode. Simulation results are in good agreement with the experiments and demonstrate a high fidelity description of the sand behaviour with the two-phase model.

Produced by

Weapons and Combat Systems Division
DST Group Edinburgh
PO Box 1500
Edinburgh SA 5111

Telephone: 1300 333 362

June 2019

APPROVED FOR PUBLIC RELEASE

Target Plate Deformation Time-History from a Detonating Buried Charge in Various Sand Media

Executive Summary

The present report expands on the analysis of the loading from a buried improvised explosive device (IED) for a variety of sands and soils, where it was considered for only dry calcite sand in a previous DST report. The momentum transfer to a target, which is important for vehicle occupant survivability, was assessed from the deformation of a target plate, which represents the vehicle floor. The target plate was subjected to loading from a high explosive (HE) charge buried under a layer of the sand/soil material. Flash x-ray was used to measure the target plate deformation and allowed for an evaluation of the momentum distribution in both space and time.

The experimental setup has been refined from the previous study and consists of a cylindrical axisymmetric configuration which can be simulated numerically in two-dimensions. This addresses limitations of the previous setup which consisted of a rectangular target plate that enabled a quasi-two-dimensional approximation, however, ultimately was still affected by the third dimension. The present setup enables validation of the two-phase sand model employed in the previous study [1] with a much higher accuracy using a two-dimensional simulation. Therefore, the two-phase sand model, implemented in the Sandia shock physics code, CTH, can be assessed with direct comparison of the experimental and numerical results without assumptions related to the physical third dimension. The comparison demonstrates a high fidelity of the modelling and high accuracy in predicting the plate deformation for the case of dry calcite sand. This prediction tool should allow for improved designs countering the threat and ultimately increase the survivability of vehicle occupants.

Various sands (and a soil) were tested with the present experimental setup, enabling an investigation of the influence of the sand parameters on the momentum transfer to the target plate. Parameters evaluated included particle size distribution, particle shape, type of sand (chemical composition), moisture content and density or level of initial compaction of the sand. This provides a sensitivity analysis on the influence of the various sand parameters which could be used to inform on the response of an unknown sand from a specific region of operation for the Department of Defence.

Authors

S. A. Weckert

Weapons and Combat Systems Division

Sam Weckert obtained a Bachelor of Engineering in Mechatronic Engineering from the University of Adelaide in 2004. He joined the Threat Mitigation Group of the Weapons Systems Division (DSTO) in 2004, and moved to the Weapons Effects Group in 2006 (now Advanced Warhead Technologies). In 2010, he spent six months working in the High Rate Mechanics and Failure Branch at the Army Research Laboratory in the US. His current areas of work include warhead terminal effects modelling, instrumentation development, and material shock response and characterisation at high strain rates.

A. D. Resnyansky

Weapons and Combat Systems Division

Anatoly Resnyansky obtained a Masters of Science in Applied Mathematics and Mechanics from Novosibirsk State University (Russia) in 1979. In 1979-1995 he worked in the Lavrentyev Institute of Hydrodynamics (Russian Academy of Science) in the area of constitutive modelling for problems of high-velocity impact. Anatoly obtained a PhD in Physics and Mathematics from the Institute of Hydrodynamics in 1985. He joined the Terminal Effects (presently Advanced Warhead Technologies) Group of the Weapons Systems Division (DSTO) in 1998. Anatoly was appointed Adjunct Professor at University of South Australia in 2014. His current research interests include constitutive modelling and material characterisation at high strain rates, and theoretical and experimental analysis of multi-phase flows. He has published over one hundred research and technical papers.

Contents

This page is intentionally blank

1. Introduction

The loading from a buried charge and subsequent momentum transfer to an aboveground target is critical for analysing vehicle survivability against landmine and buried improvised explosive devices (IEDs). Much of the work on this area in the literature focuses on integral measurements which are compounded by inertial effects and do not give any temporal information on the loading. The use of pendulum type systems typically gives a total impulse from the loading from a buried charge [1-3] (some time-history may be possible, however it is complicated by the response of the pendulum test fixture). Similarly, assessments of the residual deformation of a target plate subject to loading from a buried charge provides an integral measurement of the momentum transfer to the target, but does not give any information on the time-history of the loading. Several studies [4-5] conducted previously focused on the evolution in time of the ejecta formation from a buried charge using the flash x-ray technique. This work was extended to look at the deformation in time of a plate subjected to loading from a buried charge. The first stage of this work used a rectangular plate subjected to quasi-2D loading from an explosive charge buried in dry calcium carbonate (calcite) sand [6] and compared the plate deformation profile in time with simulations conducted using the CTH hydrocode [7], specifically incorporating [8] a two-phase material model for the sand [9].

The work presented here extends on the previous study [6] where the experimental setup has been refined to use a 2D axisymmetric setup consisting of a cylindrical charge buried within a steel cased cylinder of sand. The detonation products and sand ejecta from the detonating charge then load a disc shaped aluminium target plate and the deformation in time is again measured using flash x-ray instrumentation. The 2D axisymmetric setup allows for easier comparison with simulation studies conducted in the CTH hydrocode [7], whereby a more finely resolved mesh can be used in 2D compared to the 3D case. Two loading conditions, using different initiation (point versus planar initiation) of the main charge were used in the experiments. This provided different temperature and pressure conditions within the sand and a different spatial loading on the target plate, thus allowing for a more robust evaluation of the two-phase material model developed for the sand in the CTH simulations.

A further extension of the previous testing was that for this series of experiments multiple sands were tested. The different sands were specifically chosen to vary the sand morphology, considering parameters such as particle shape, particle size distribution, type of sand (chemical composition), moisture content and compaction. An example soil/ roadbase mix was also tested. The aim was to assess the sensitivity of these different variables and investigate their effect on the loading and subsequent target response. Ultimately, from a practical standpoint this could allow the Department of Defence to compare soil samples taken from areas of operation with soils that have known responses. This is obviously a very complex task, but the variables assessed here represent a first step in this endeavour.

Complementary to this is the ability to model the sand or soil response, based on measurable characteristics and additional characterisation tests specific to the type of the

loading. Here, for one of the sands tested (dry, uncompacted calcium carbonate sand), the two-phase material model for the sand has been evaluated for its ability to accurately predict the subsequent loading to an above ground target. The two-phase model incorporates high strain rate compaction data from Split Hopkinson Pressure Bar (SHPB) tests (detailed in [10]). It also incorporates a sintering kinetic equation for capturing transformations within the material during the loading, which is tuned from explosively loaded capsule tests (detailed in [11]). The two-phase model takes into account energy dissipation mechanisms not captured by traditional models and is shown to provide a more accurate description of the loading to a target. Here, the goal is to establish a methodology for appropriately characterising a sand or soil under high pressure, high strain rate explosive loading conditions, such that the loading to a target can be accurately modelled. Example applications for the modelling can then include vehicle vulnerability assessments to buried improvised explosive threats from a country/area specific ground type and the ability to then use simulation studies to develop appropriate protection measures.

2. Methodology

2.1. Experimental Setup

A schematic of the general experimental setup is shown in Figure 1 (left), where the setup is radially symmetric about a central axis. The setup consisted of a cylindrical high explosive charge buried inside a steel container and an aluminium target plate at a fixed standoff from the top of the sand. When the explosive detonates, initially a shock wave travels through the surrounding sand which may cause material transformations within the sand at the microstructural level. Following this, the high pressure detonation products expand and push the surrounding sand upwards to form an ejecta. The combined sand ejecta and detonation products load the target plate, deforming it in the early stages (potentially until it breaches) and causing gross motion of the plate or plate fragments in the later stages. The focus here is on the early stages of loading characterised by the initial target plate deformation in time.

The steel container has an internal diameter of approximately 430 mm and wall thickness of 12.7 mm and the steel base is 40 mm thick (Figure 2). The volume of sand is approximately 20 L and is screeded level with the top of steel cylinder. The target plate rests on top of wooden supports at a standoff of 100 mm from the top of the sand surface. It has a diameter of 500 mm, with thickness of 4 mm and made from 6061-T6 aluminium.

The instrumentation for measuring the plate deformation consisted of flash x-ray from the side. Additionally, there are two high speed cameras looking down from the top, giving a stereoscopic image of the plate deformation. The flash x-ray setup consisted of 2 × 300 kV and 2 × 600 kV pulsers which exposed three cassettes positioned radially around the target plate as shown in Figure 1 and 2 (right). The two 300 kV pulsars utilised remote heads positioned side by side which double exposed the corresponding cassette. All four x-ray pulsars were fired at different times, giving the plate deformation as a progression in time.

For the majority of the tests, the times were 300 μs, 350 μs, 400 μs and 500 μs after functioning of the detonator.

The two high speed cameras were positioned at the top windows of the explosive test chamber, looking down onto the top of the aluminium target plate, with flash bulbs used for illumination. The plate was spray painted matt white and then speckled with matt black paint to produce a random speckle pattern. This was in order to use the Digital Image Correlation (DIC) technique for calculating the 3D plate deformation from the stereoscopic high speed video images. Unfortunately, problems with the camera synchronisation (which were not realised until late in the test program) prohibited useful data being obtained with this technique.

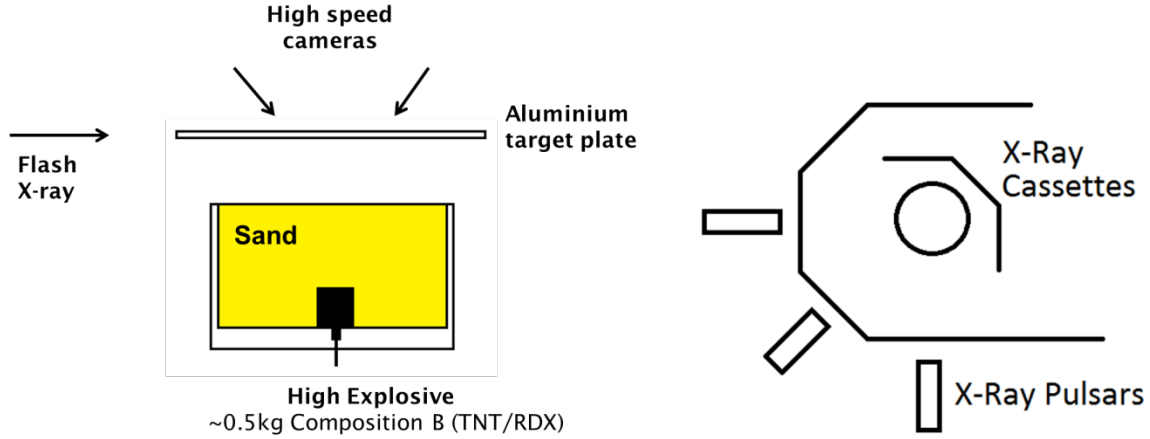

Figure 1 - Schematic of the experimental setup; buried charge and target plate (left), and chamber setup with instrumentation (right)

Figure 2 - Experimental setup; inside explosive chamber (left), and outside chamber showing x-ray pulser units (right)

Two charge configurations; differing in the method of initiation of the main explosive charge, were used for the testing. The main explosive charge for both setups was a 73 mm diameter by 73 mm height cylinder of Composition B (60% RDX 40% TNT) with a mass of 515 g.

For Configuration A (Figure 3), the main charge was end initiated, centrally on the bottom face of the charge, using a 20 mm diameter by 20 mm height pentolite booster (mass of 10.8 g) and RP80 exploding bridge wire (EBW) detonator. This point initiation results in a curved detonation wave travelling through charge and some degree of divergence of the explosive energy into the surrounding sand.

For Configuration B (Figure 3), the main charge was initiated from underneath using an explosive plane wave generator which added an additional 330 g of explosive. This simultaneously initiates the entire cylinder end and results in a planar detonation wave propagating through the main charge, and a nearly planar loading on the sand above. The planarity of the charge was assessed and validated experimentally. The explosive plane wave generator was constructed using explosive lensing, using two speeds of explosive to tailor the shape of the detonation wave. It consisted on a TNT solid inner cone (the slow explosive, mass of 102 g) surrounded by a Composition B outer cone (the fast explosive, mass of 228 g). The angle of the cones is dictated by the ratio of the velocity of detonations of the explosives. The cone apex was initiated using a 12.7 mm diameter by 12.7 mm height Composition TR1 booster (mass of 2.6 g) and smaller RP87 EBW detonator.

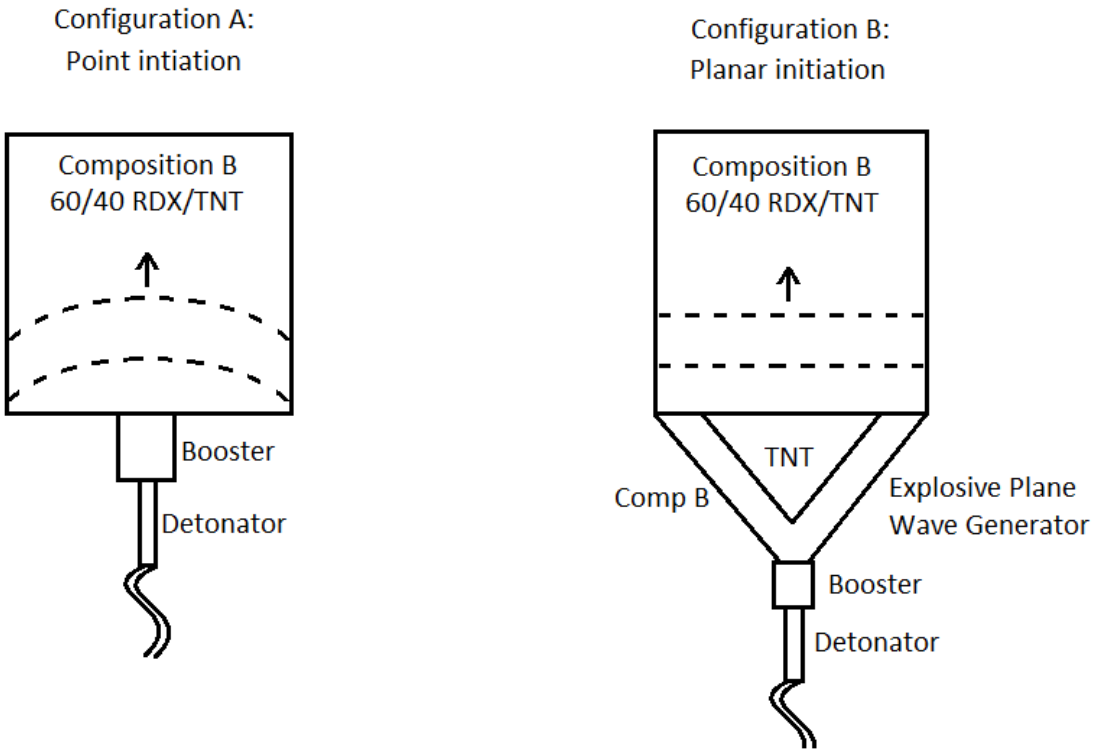

Figure 3- Schematic of charge configuration A (left) and charge configuration B (right)

The two different charge initiation configurations provides different temperature and pressure loading conditions on the surrounding sand, which influences possibly shock consolidation (sintering) within the sand, and affects the ejecta formation and loading on the target plate.

2.1.1. Materials

The materials used for burying the explosive charge were selected to vary specific variables regarding the sand morphology, which may have an influence on the resulting loading to the target plate. The variables included the particle size distribution (fine *vs* coarse particles), particle shape (spherical vs naturally angular/irregular shapes) and chemical composition (silica vs calcium carbonate based sands).

The mechanical/physical properties of the sand such as size and shape were expected to influence the inter-particle interactions and the chemical composition was expected to be important for possible sintering effects via the melting temperature for the material. Packing density and moisture content (dry vs wet) was also investigated. The packing density and specifically the air trapped between the particles was considered important for possible sintering effects, where the trapped air is expected to undergo adiabatic compression under the shock loading conditions, leading to hot spots between the particles. This was explored by including diatomaceous earth as a test material which is a highly porous, silica based naturally occurring material with a very intricate structure and high surface area. An example soil, a road base material, was also included in addition to the sands and silica based materials discussed above. The road base represents a real material with complexity in its composition. Scanning Electron Microscopy (SEM) images of the materials tested are shown in Figure 4.

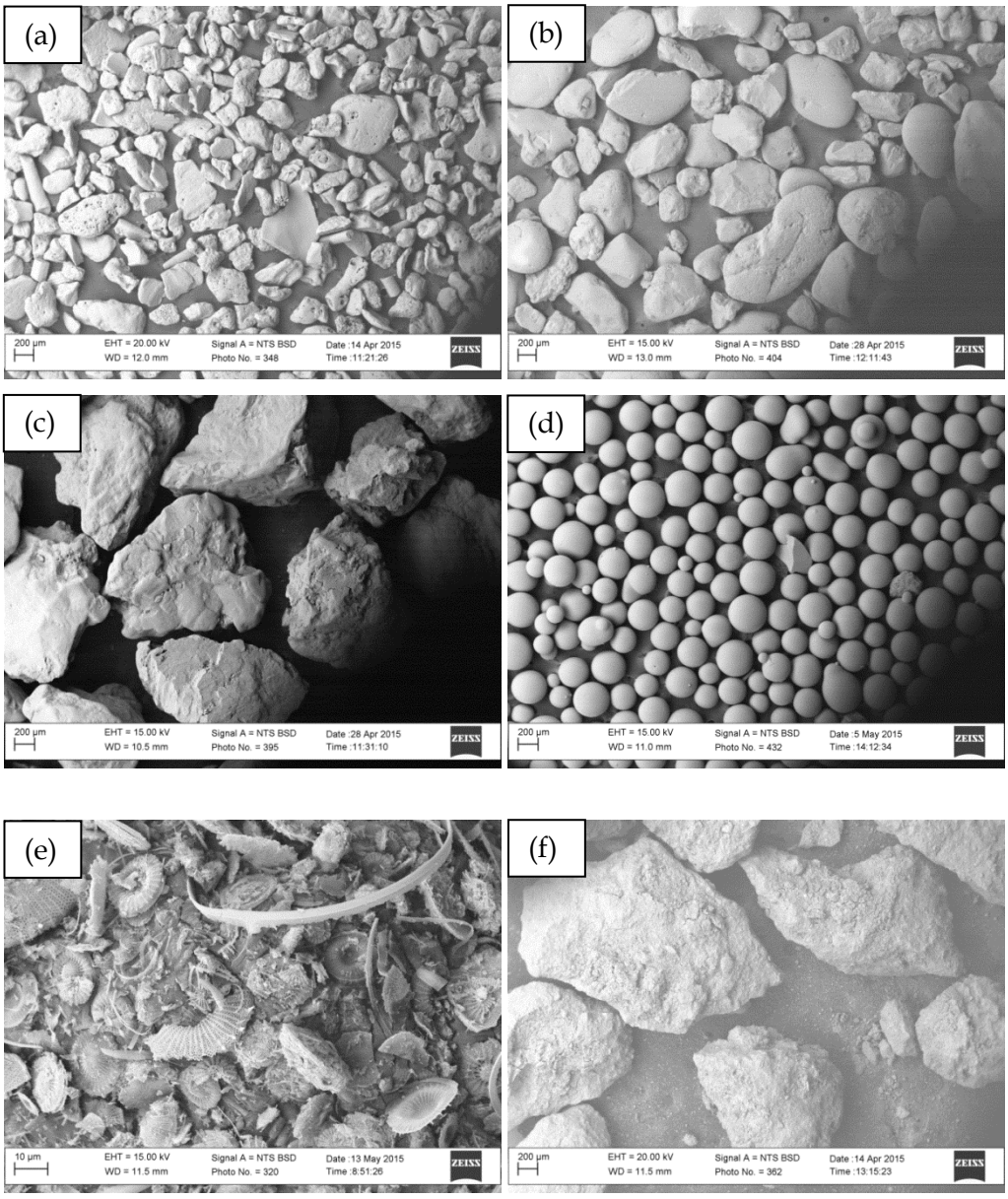

Figure 4- Scanning Electron Microscopy (SEM) images of the materials: (a) calcium carbonate sand, (b) silica sand, (c) coarse silica sand, (d) glass beads, (e) diatomaceous earth, (f) road base.

The particle size distribution, as determined by a sieve analysis, is shown in Figure 5 for the calcium carbonate ("Richgro Washed Playsand") and silica based sands. The silica (quartz) sand ("Tuscan sand") was chosen to give a similar particle size distribution to the calcium carbonate sand and the second coarse silica sand ("Unicorn Filter sand") gives a shift in the particle size distribution to the right. The SEM image of the calcium carbonate sand (Figure 4 (a)) shows some porosity within the individual grains. This sand is a limestone based material and is also sometimes called 'coral sand'. In comparison the grains of the silica sands (Figure 4 (b) and coarse (c)) appear relatively solid and non-porous.

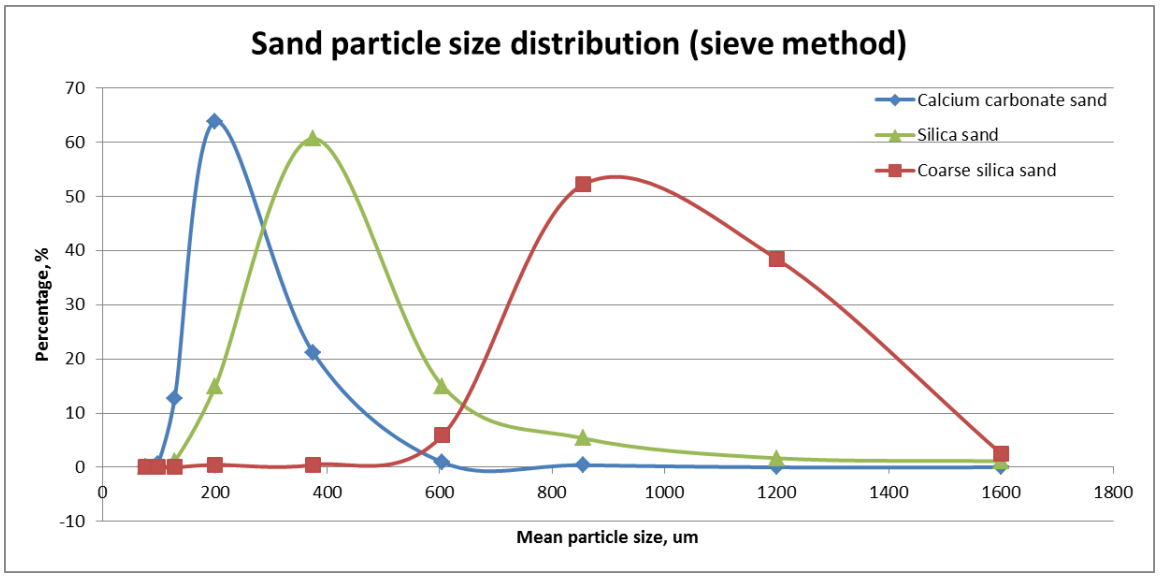

Figure 5- Particle size distribution for sand materials

The solid glass beads (Figure 4 (d)) are manufactured from soda lime glass. They represent an artificial sand which has spherically shaped smooth particles comprised of an amorphous silica based material. Thus some comparison is possible with the naturally occurring silica sand, where the particle shape is more angular. However, the glass beads are amorphous silica based (soda lime glass) whereas the silica sand is polycrystalline silica (quartz) so the chemical composition and particularly the crystallinity differs also. The glass beads were purchased as industrial grade sand blasting beads (supplier: Abrasive Blasting Service and Supply), in two sizes: 250-425 µm and 180-300 µm. A mix of 75% 250-425 µm and 25% 180-300 µm was made to roughly approximate the particle size distribution of the silica sand.

Table 1 - Summary of properties of the test materials

Test#	Material	Composi-tion	Ave Particle size, µm	Bulk density ** g/cm³	Crystallinity
	Calcium carbonate sand	$CaCO_3$	200		55%
A8, B1	Dry			1.31 (A); 1.33 (B)	
A2, B4	Dry, Compacted			1.49 (A); 1.45 (B)	
B9	10% moisture			1.21 (B)	
	Silica sand	SiO_2	375; >1000 sieved out		100%
A3, B2	Dry			1.57 (A); 1.57 (B)	
A6, B8	10% moisture			1.59 (A); 1.58 (B)	
	Coarse silica sand	SiO_2	850		79%
A4, B3	Dry			1.54 (A); 1.44 (B)	
A7, B7	10% moisture			1.55 (A); 1.41 (B)	
A5, B5	Glass beads (soda lime glass)	SiO_2 + Na_2O, CaO + …	75% of 250-425 25% of 180-300	1.54 (A); 1.48 (B)	Amorphous
B6	Diatomaceous Earth	~SiO_2		0.14 (B)	Amorphous
B10	Road base 7.4% Moisture	Complex mix	75 - 25000	2.05 (B)	28%

** The measured bulk density (calculated from mass of sand/volume for each test)

The diatomaceous earth (Figure 4 (e)) is a naturally occurring, amorphous, silica based material. It has a very intricate structure as shown in the SEM image, which leads to a very large surface area, low bulk density and consequently a large amount of air within the material. It was purchased under the commercial name "Celite S" and supplied in a dried state. The road base mix consisted of a complex mineral mix with particle size distribution from 75 µm up to large aggregate 25 mm in size. The properties of all the test materials, including: chemical composition, average particle size, packing (bulk) density and particle crystallinity (as determined by QXRD analysis), are summarised in Table 1.

3. Experimental Results

The general state of the explosive chamber post-test is shown in Figure 6 (left), with the initial pre-test set-up shown in Figure 2 (left). The x-ray cassettes can be seen still standing and are opened for subsequent digital scanning and analysis. The recovered target plate fragments are shown in Figure 6 (right), and show the centrally focussed loading from the combined ejecta and explosive detonation products which causes failure and petalling of the plate at the later stages on the deformation.

Figure 6 - Explosive chamber post-test (left); and recovered target plate fragments (right)

The main metric from these tests is the target plate deformation (magnitude and shape) as a function of time. Additional information can also be extracted from the x-ray images such as the ejecta shape which can be important for assessing directionality of the loading in modelling validation studies.

An example of the flash x-ray images is shown in Figure 7 corresponding to test A5: charge configuration A, glass beads, dry, ρ=1.54 g/cm^3. Notice that the top left image has been double exposed at 300 and 400 µs. The two images are shifted horizontally due to the two remote heads for the flash x-ray source positioned side by side, thus the source origin is not the same.

All of the flash x-ray images are provided in Appendix A where they have been superimposed with a vertical scale image taken prior to the test, with scale graduations every 10 mm for referencing the plate centre deformation. An example is shown in Figure 8 for calculating the plate deformation at 400 µs. These deformation values are subsequently used for the comparison graphs in the following section.

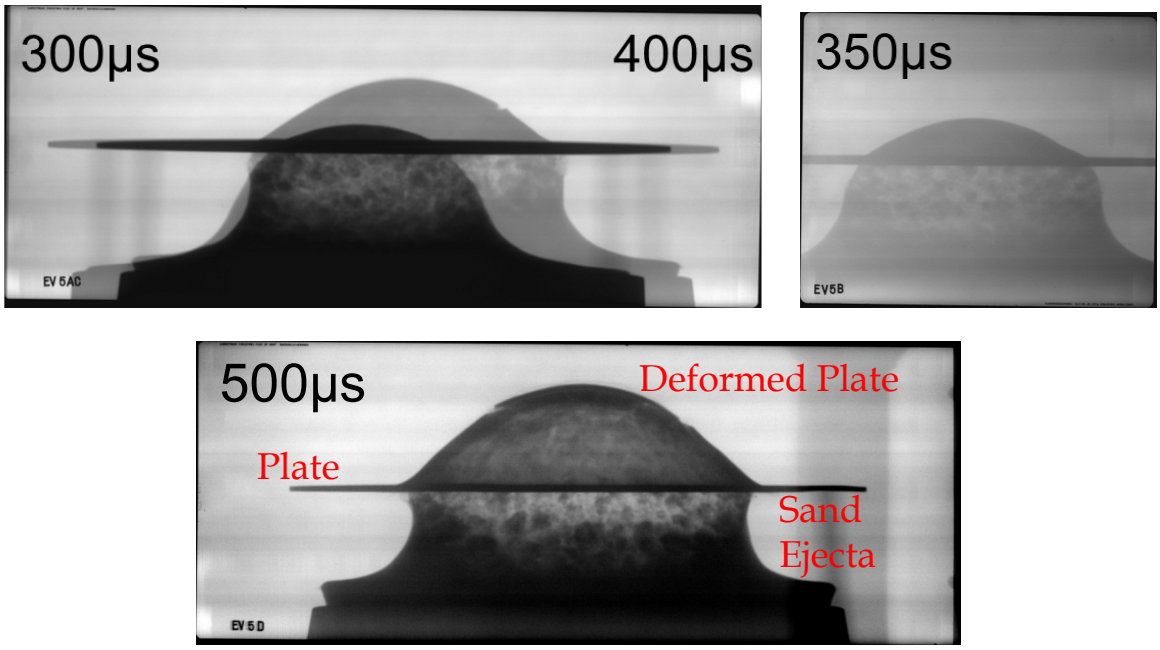

Figure 7 - Flash x-ray images at 300, 350, 400 and 500 µs for test A5 - charge configuration A, glass beads, dry, ρ = 1.54 g/cm³ (the top left image shows the x-ray cassette double exposed at two different times by the two remote head x-ray pulsars)

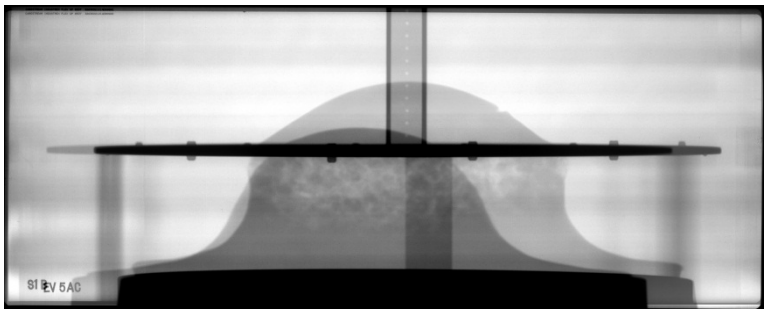

Figure 8 - Flash x-ray image for test A5, where a vertical scale imaged prior to the test has been superimposed on the deformed plate image for calculating the plate centre deformation at 400 µs

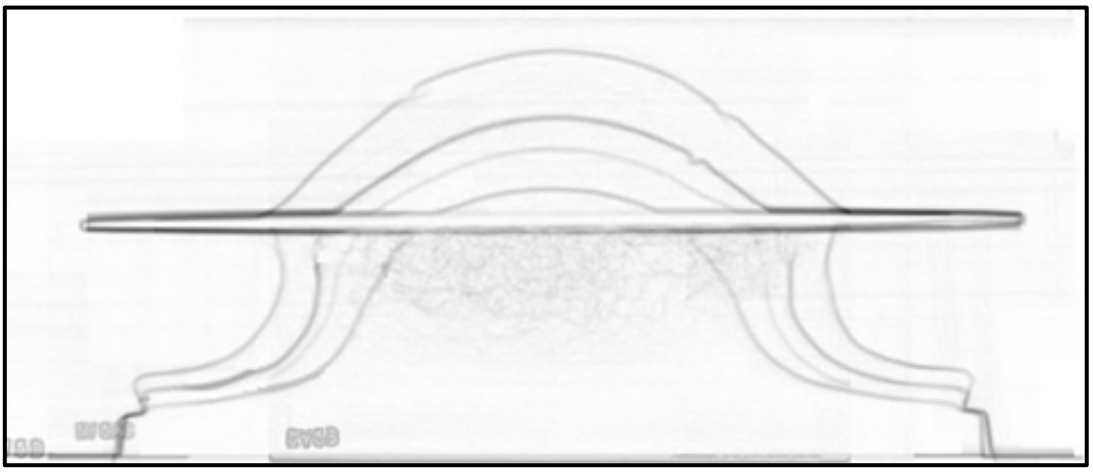

Figure 9 – Superimposed and thresholded flash x-ray images for test A5 showing the evolution of the plate deformation and ejecta loading in time

An evolution of the plate deformation in time for test A5 is shown in Figure 9, where the experimental plate profiles at 300, 350, 400 and 500 μs are superimposed onto a single image. The evolving profile of the ejecta field loading the plate can also be seen and provides additional information for modelling validation and development.

An important thing to notice from the flash x-ray images is that the plate deformation occurs early on in the loading from the combined sand ejecta and detonation products, before any gross motion of the plate upwards. This is seen in the x-ray images where the plate (which only rests on top of wooden supports) remains stationary at the edges during the early time over which the deformation occurs (no vertical adjustment to the image superposition has taken place).

The plate deformation at the centre of the plate, as an evolution in time, is shown in Figure 10 for the Configuration A tests. The dry fine silica sand (ρ = 1.57 g/cm^3), coarse silica sand (ρ = 1.54 g/cm^3) and glass beads (ρ = 1.54 g/cm^3) all give very similar results and have the least plate deformation at a given time. The grouping of these three tests, suggests that the particle size does not have a significant influence on the result (fine silica sand versus coarse silica sand) and that the particle shape may not be too influential either for the plate deformation metric measured here. This is evidenced by the similar results for the fine silica sand, which is naturally angular, versus the glass beads, which are round, smooth and nearly spherical. The densities are all the same (within several percent) for these three tests and all have no moisture content, making it somewhat easier to isolate the variables of particle size and particle shape.

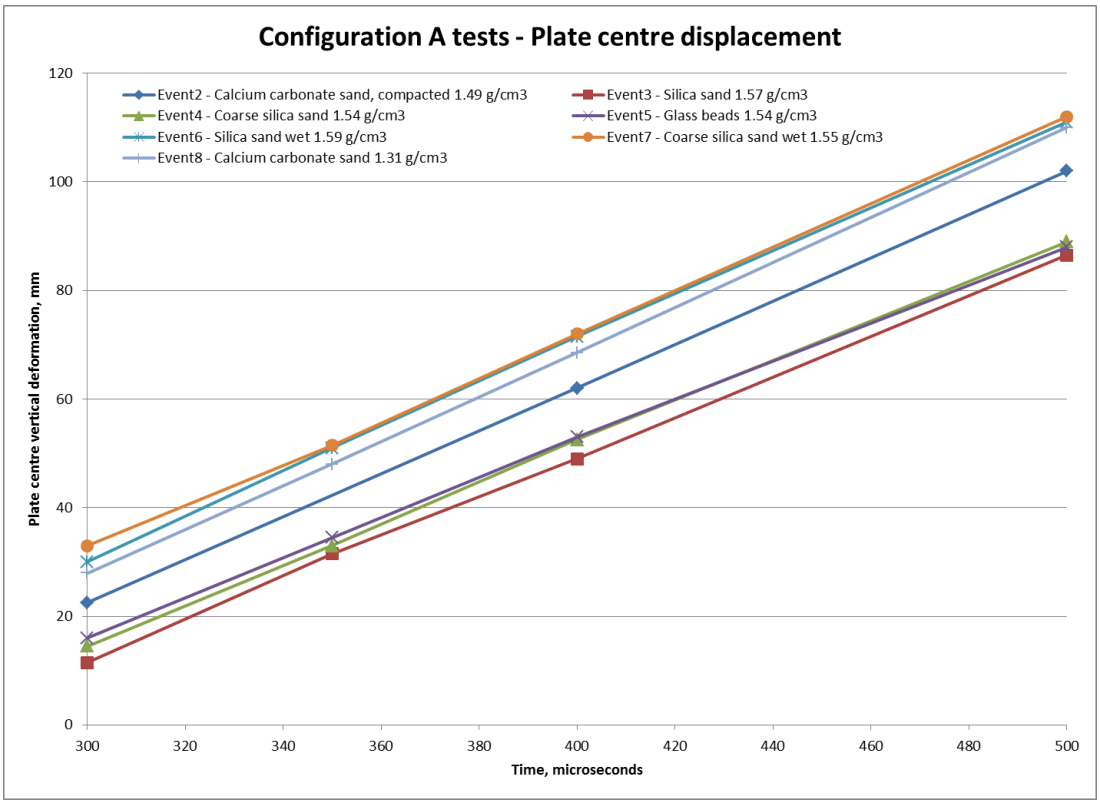

Figure 10 - Plate deformation evolution in time for the Configuration A tests

The dry calcium carbonate sand had a higher deformation at a given time compared with the silica based sands, suggesting an influence of the chemical composition on the sand, however this test was also at a significantly lower bulk density (ρ = 1.31 g/cm^3). The same sand, in a compacted state (ρ = 1.49 g/cm^3), produced a lower deformation, highlighting the importance of bulk density as an influential variable for the results. However, the deformation was still higher than the silica based sands (ρ = 1.54 g/cm^3 and ρ = 1.57 g/cm^3). So whilst the silica sand tests had a slightly higher bulk density, the chemical composition of the sand (silica versus calcium carbonate), and potentially the material density of the actual particles, appear to be important factors that also influence the results. The chemical composition aspect is important for the possibility of sintering occurring through a process of shock consolidation; whereby the melting temperature of the sand plays an important role and is dependent on the chemical composition of the sand (~1700 °C for crystalline quartz silica and between 800 - 1300 °C for various crystalline forms of calcium carbonate).

The introduction of water, 10% by weight, to the fine and coarse silica sands resulted in a consistent and significantly higher deformation at a given time compared to the equivalent dry silica sand tests. This shows that the plate deformation, and overall momentum transfer to the plate, is heavily influenced by the moisture content in the sand and it is shown here to be the most influential variable out of the five variables explored. The wet fine silica sand (ρ = 1.59 g/cm^3) and wet coarse silica sand (ρ = 1.55 g/cm^3) gave almost identical results. This is consistent with that seen for the equivalent dry tests, and supports

the argument that the particle size is not an influential variable for the metric of plate deformation measured here, possibly because the particle breakage, compaction and sintering effects occur before the plate loading, however these mechanisms are still relevant to the energy dissipation and resulting resistance to deformation of the ejecta.

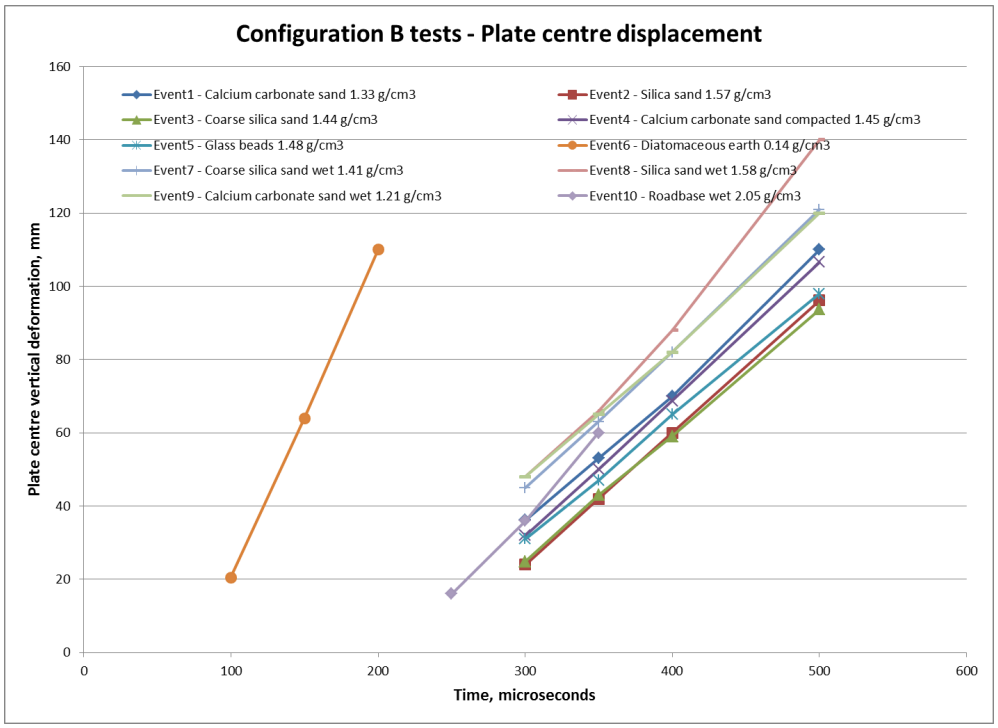

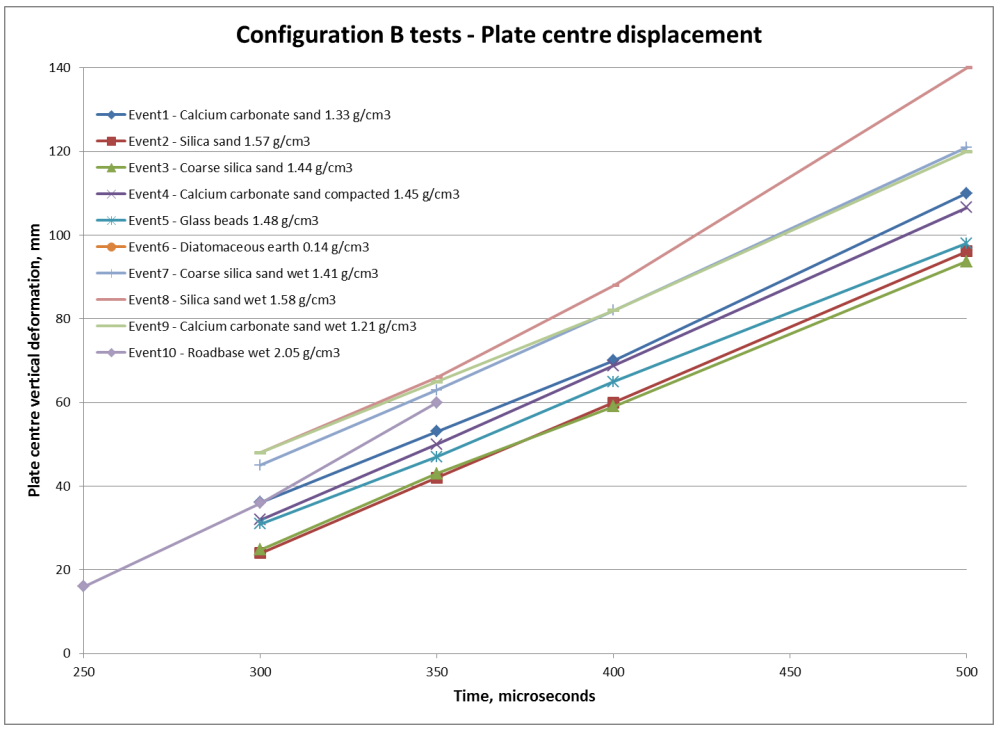

Figure 11 - Plate deformation evolution in time for the Configuration B tests, where the bottom graph is a zoomed portion (excluding the diatomaceous earth test) of the top graph

The plate deformation, at the centre of the plate, as an evolution in time is shown in Figure 11 for the Configuration B tests. The trends are very consistent with that seen in Figure 10 for the Configuration A tests. The dry fine silica (ρ = 1.57 g/cm^3) and coarse silica (ρ = 1.44 g/cm^3) sands have almost identical response and give the least plate deformation at a given time. They are both crystalline silica naturally occurring sands, but differ in their average particle size and also different bulk/packing density for the tests here. The dry calcium carbonate sand had a higher deformation at a given time and is slightly higher in the uncompacted state (ρ = 1.33 g/cm^3) compared with the compacted state (ρ = 1.45 g/cm^3). The plate deformation from the glass beads was in between that for the dry silica and calcium carbonate sands. The introduction of water to the sands, 10% by weight, resulted in a consistently higher deformation at a given time compared to the dry sand tests.

The wet coarse silica and wet calcium carbonate sands gave almost identical results, and the wet fine silica sand was slightly higher. The road base (ρ = 2.05 g/cm^3) with 7.5% moisture gave a lower deformation at early time compared with the other wet sands in tests B7 - B9 (which had a lower density), however appeared to have larger velocity and resulted in a higher deformation at a later time for this test. Particularly the different slope of the deformation curve reflects the significantly different material type for the road base compared with the various sands. The flash x-ray timings for road base test were set earlier at 200, 250, 300 and 350 µsec, however the soil ejecta and detonation products had not yet hit the plate at 200 µsec, giving only three data points for this test.

The diatomaceous earth also represents a significantly different material from the other materials tested. It is silica based (amorphous), however its very low bulk density (ρ = 0.14 g/cm^3) and large amount of air within the material makes the response and loading to the target plate substantially different to the other tests. The results for the diatomaceous earth test are shown in the top graph of Figure 11, where the plate deformation curve lies in a different area of the graph, away from the grouping of results from the rest of the tests. There is less mass to be accelerated during the ejection process, so the ejecta and driving detonation products arrive at the target plate much earlier and at a higher velocity. This is reflected in the plate deformation, however, the loading is more localised to the centre of the plate and hence the shape of the deformation is significantly different to the other tests.

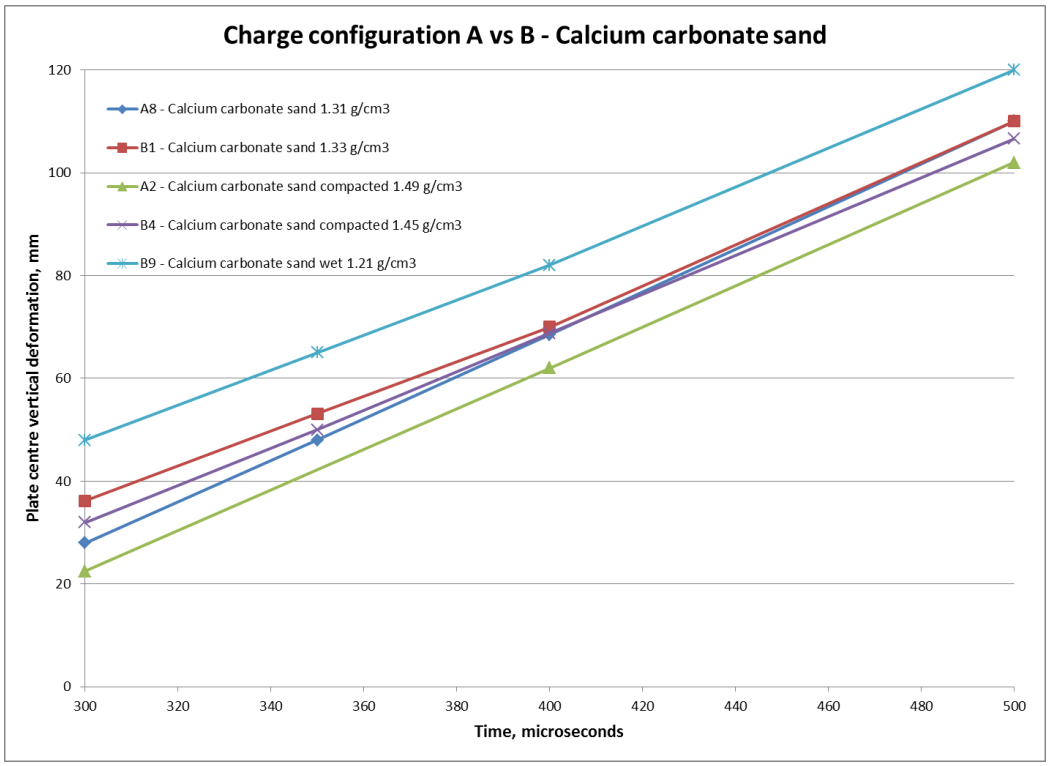

Figure 12 - Plate deformation evolution in time: effect of explosive charge initiation (calcium carbonate sand)

The effect of the explosive charge initiation on the results is shown in Figures 12 – 15 for the different sand types. The charge configuration A tests use a point initiation of the main charge, whereas the charge configuration B tests use an explosive plane wave generator to simultaneously initiate over the cylinder end. This results in a difference in the geometric nature of the energy release. The point initiation causes a curved detonation wave to propagate through the charge and the explosive energy is released radially as well as axially from the cylindrical main charge. Whereas, the plane wave generator cause a planar detonation wave to propagate through the explosive cylinder and so the axial energy output from the top of the cylinder is stronger and overall the energy is more focussed upwards, approximating more of a 1D planar loading on the sand above. This stronger, more focussed loading exposes the sand to different pressure and temperature conditions, compared with the point initiated charge.

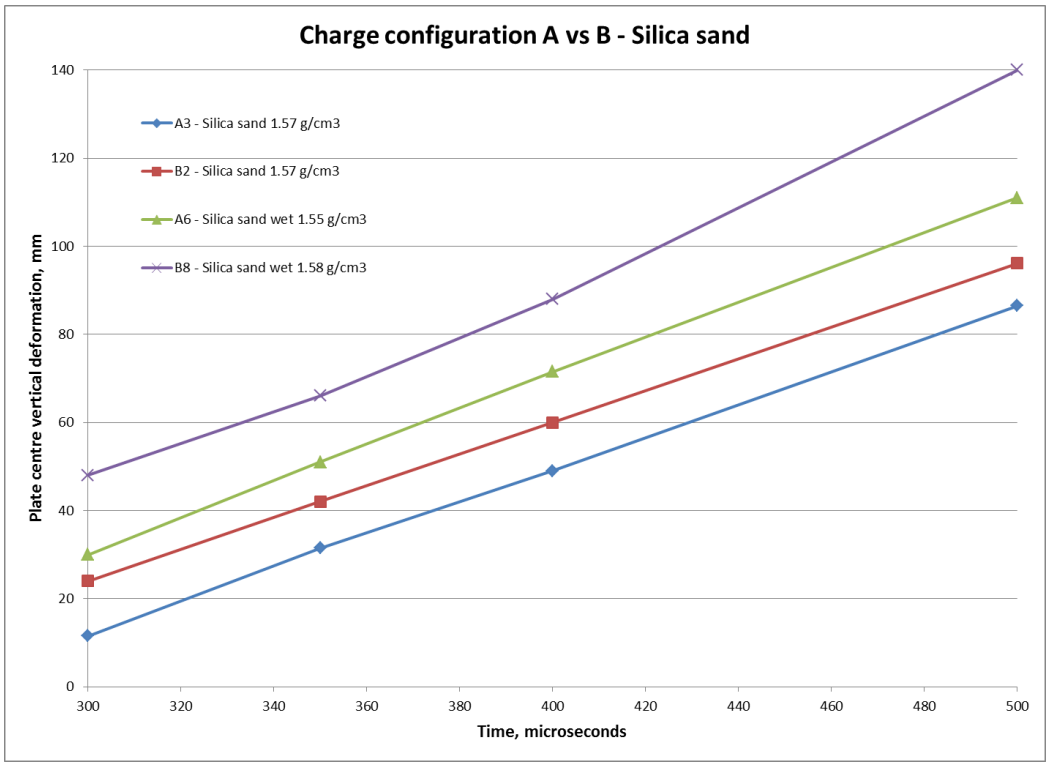

Figure 13 - Plate deformation evolution in time: effect of explosive charge initiation (silica sand)

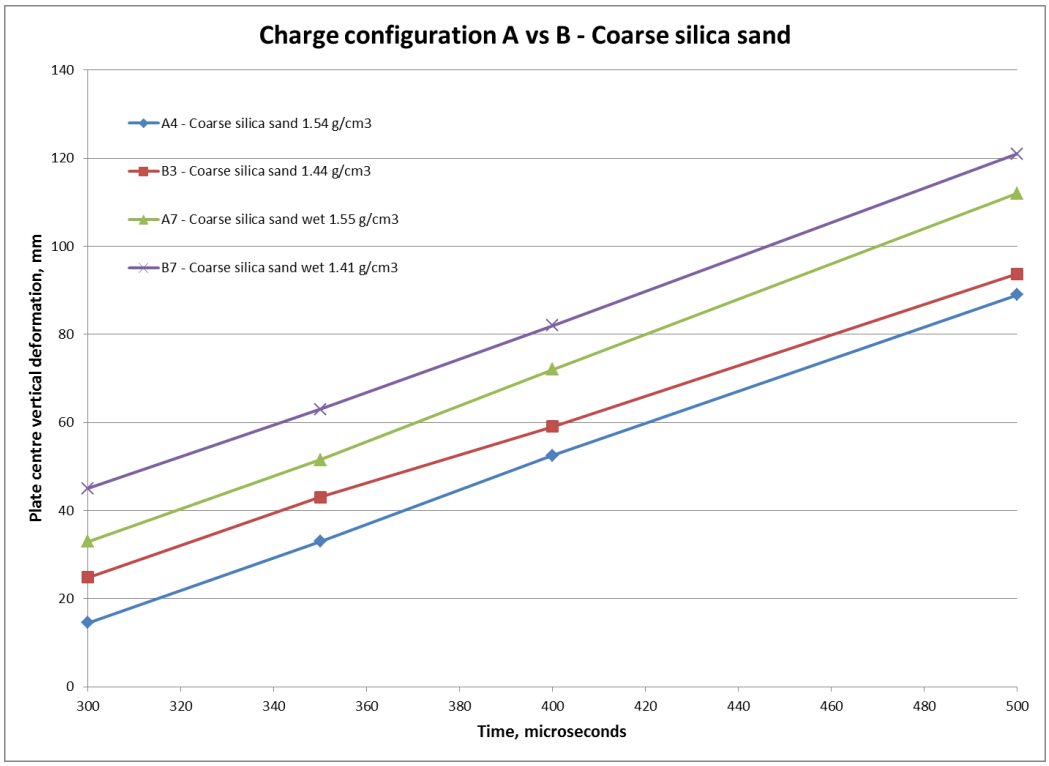

Figure 14 - Plate deformation evolution in time: effect of explosive charge initiation (coarse silica sand)

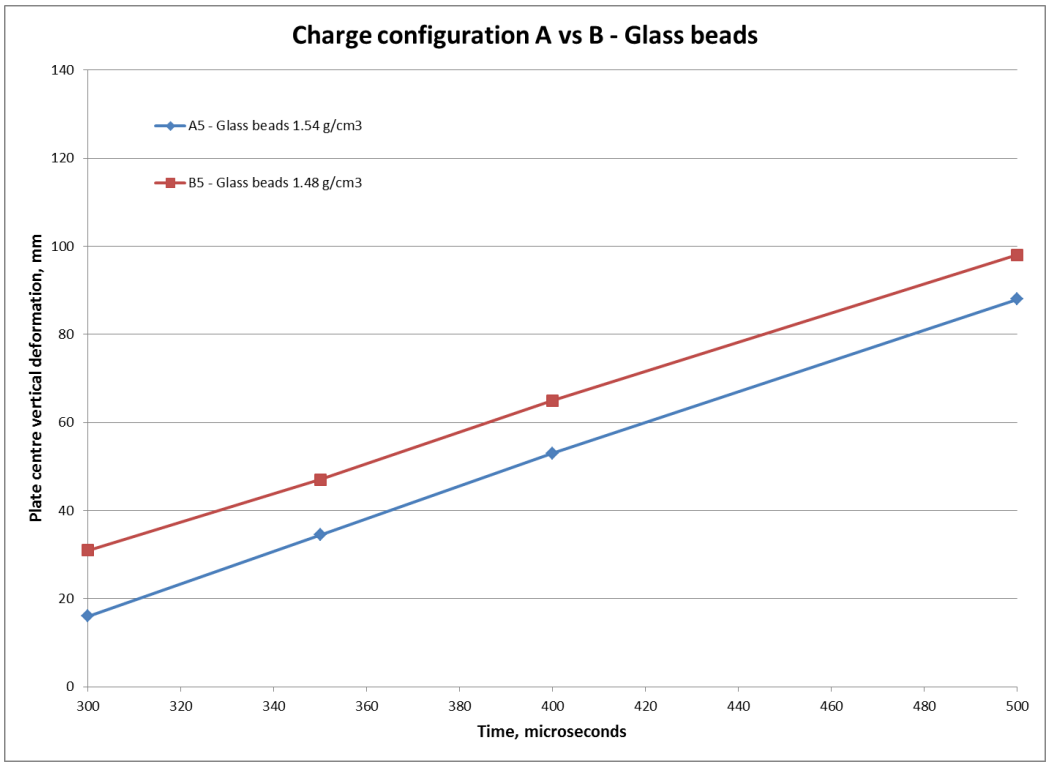

Figure 15 - Plate deformation evolution in time: effect of explosive charge initiation (glass beads)

The main charge, a 73 mm diameter by 73 mm height cylinder, of mass, 515 g is the same for both charge configurations. However, in the case of charge configuration B the explosive plane wave generator increases the total explosive content overall (additional 330 g) and energy available to deform the plate. The other important difference between the two charge configurations is the flash x-ray timings. In both cases the flash x-ray times are referenced to the detonator functioning at time zero. However, the additional time required for the detonation wave to propagate through the explosive plane wave generator (a two component conical charge on the end of the cylindrical main charge) means that the onset of detonation of the main charge is now at a slightly later time. Consequently the plate deformation times are in effect slightly earlier compared to the configuration A tests. Considering the length and speeds of the explosive used in the plane wave generator, the time difference is approximately 10 µsec.

Given these points, the plate deformation results in Figures 12 - 15, consistently show a higher plate deformation for the charge configuration B tests. This difference would be further increased if accounting for the 10 µsec offset discussed above, effectively shifting the plotted data points to the left slightly. The higher plate deformation is consistent with the increased explosive content. However the benefit of conducting these two different test variants is that the different initiation techniques result in different spatial distributions of the explosive energy and expose the sand to different pressure and temperature conditions. As validation data for a numerical model of the sand behaviour, this assesses the model under different conditions for a more thorough assessment. It should be noted that for the configuration B tests for the coarse silica sand (Figure 14), the density was

lower for both the dry and wet tests compared to the configuration A tests, owing to some batch variation in the sand. However the trend of a higher plate deformation at a given time for the configuration B tests was still evident, and consistent with the results for the other materials.

The previous graphs highlighted the differences in the plate maximum centre deformation from the two different charge configurations, however the width and shape of the deformation is also an important aspect. As discussed previously, the point initiation of the main charge used for the Configuration A tests results in a convex detonation wave travelling up through the main charge with subsequent geometric spreading and dissipation of the explosive energy. Whereas, the plane wave initiation of the main charge for the Configuration B tests, results in a more focussed output of the explosive energy upwards. For the uncompacted calcium carbonate sand, both charge configurations gave a final plate centre deformation of 110 mm at 500 µsec. The x-ray images of the plate deformations are shown in Figure 16 for the configuration A and configuration B tests. There is a subtle difference in the plate deformation between the two tests, specifically at the edge of the deformation.

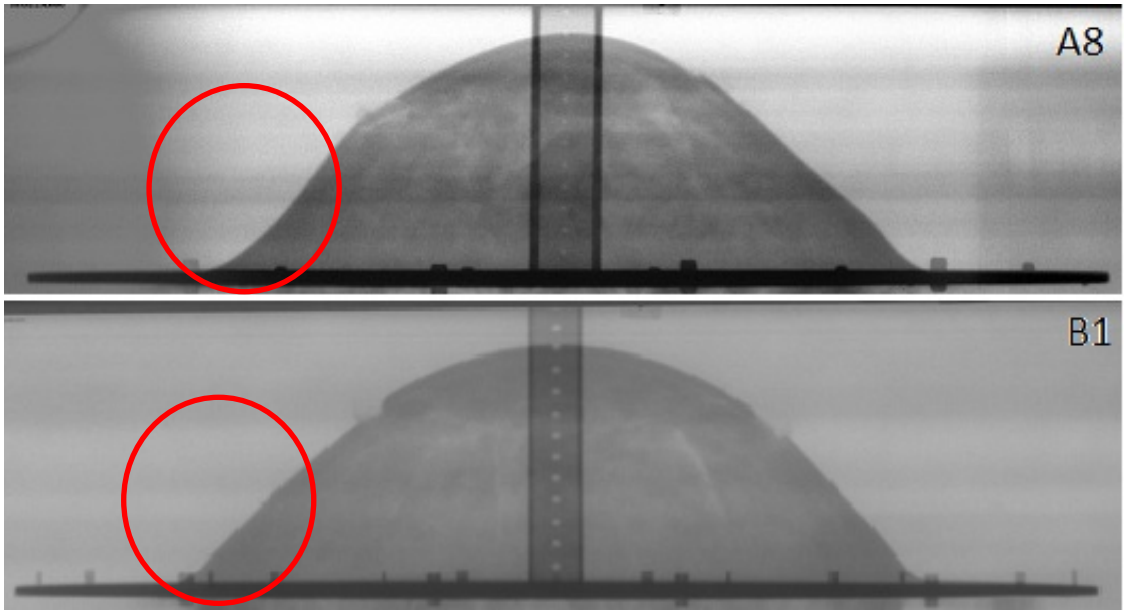

Figure 16 – Comparison of plate deformation profiles at 500 µsec for Test A8 - calcium carbonate sand, configuration A charge (point initiation) and Test B1 – calcium carbonate sand, configuration B charge (plane wave initiation).

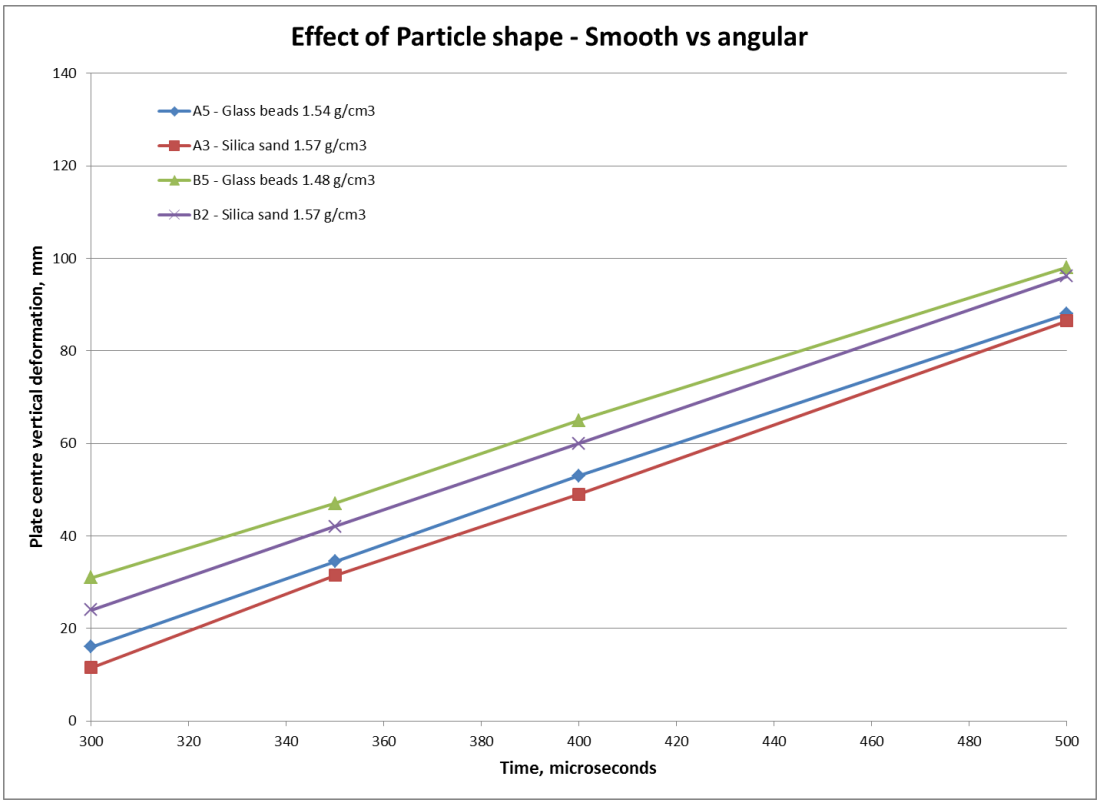

Figure 17 - Plate deformation evolution in time: effect of particle shape

The effect of particle shape on the results is shown in Figure 17. For both the Configuration A tests (A3 and A5) and the configuration B tests (B2 and B5), the smooth and round glass beads consistently give a higher plate deformation result compared with the natural angular shaped silica shape. For the Configuration A tests, the densities are very similar (within several percent), however for the Configuration B tests there is a larger disparity in bulk density which complicates the comparison. Additionally, the round glass beads and angular silica sand particles are not from an identical material. Both are silica based, however the glass beads are soda-lime glass which is amorphous in structure, whereas the silica sand is a natural silica sand which is polycrystalline in its microstructure. These points should be taken as a caveat to the comparison presented here looking at the effect of particle shape, nevertheless it appears that the effect of particle shape is small.

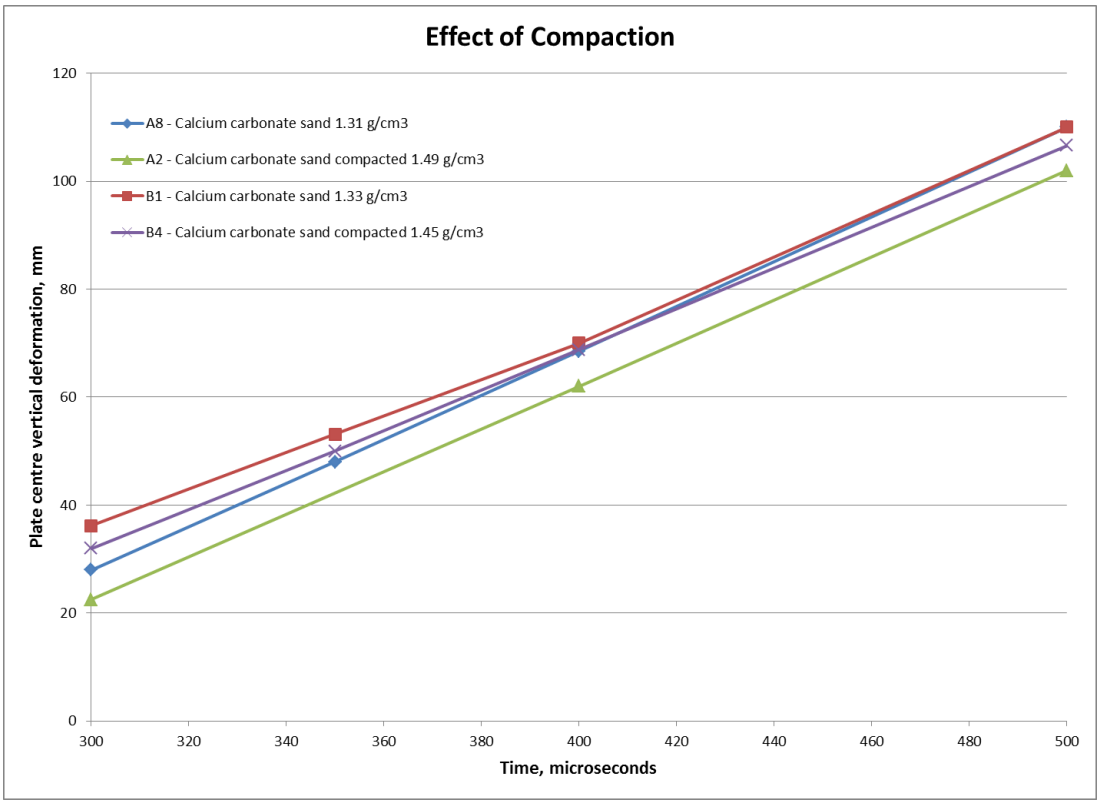

Figure 18 - Plate deformation evolution in time: effect of compaction (bulk density)

The effect of compaction (or the bulk density of the sand) on the results is shown in Figure 18. For the charge Configuration A tests (A8 and A2) the plate deformation is distinctly lower for the compacted state. Here, the density of the sand is increased by 14% (1.31 to 1.49 g/cm^3) for these tests.

For the Configuration B tests (B1 and B4) the results are consistent with before, where the plate deformation is lower for the compacted state, however it is less pronounced in this case. Here the density difference is less (1.33 to 1.45 g/cm^3 = 9% increase) and this smaller change in density is reflected as a smaller difference in the plate deformations in the results.

Thus, these tests suggest that the level of compaction, and corresponding bulk density of the sand, is an important variable for the metric of plate deformation here.

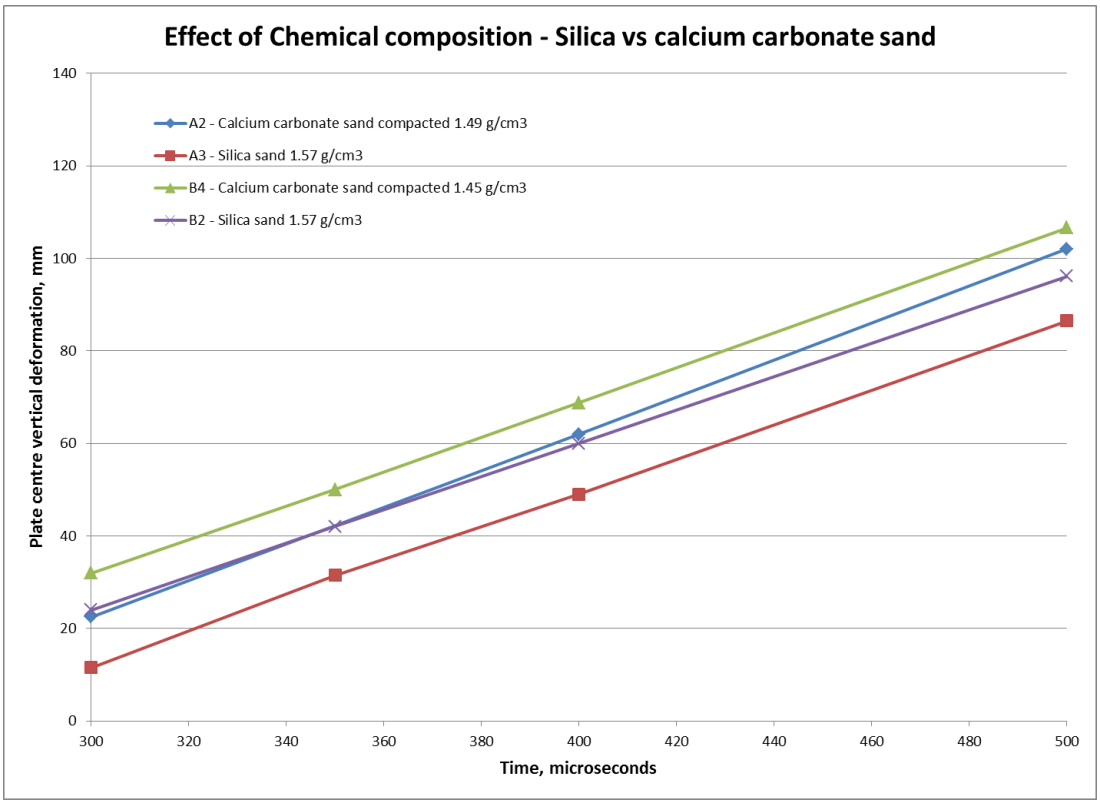

Figure 19 - Plate deformation evolution in time: effect of chemical composition

The effect of chemical composition of the sand on the results is shown in Figure 19. For both the Configuration A tests (A2 and A3) and the Configuration B tests (B2 and B4), the calcium carbonate sand results consistently had a larger plate deformation compared with the silica based sand. However, there is also some bulk difference in density between these two materials, which makes it difficult to completely isolate the variable of sand chemical composition. Still, the difference observed between the calcium carbonate and silica sand results is larger than that from the compaction results in the previous section (Figure 18), indicating that the chemical composition has an influence on the results. The detonation process of the high explosive exposes the surrounding sand to very high pressures and temperatures, thus potentially causing the material to undergo a chemical reaction. Hence, it is not surprising that the type of sand is important. Calcium carbonate can potentially undergo a decomposition reaction to calcium oxide and carbon dioxide gas. Silicon dioxide is more chemically stable than calcium carbonate, however it can still melt at higher temperatures (melting point of 1713 °C for quartz vs 1339 °C and 825 °C for the calcium carbonate crystalline forms: calcite and aragonite, respectively) and this raises the possibility of sintering between the sand grains through a process of shock consolidation.

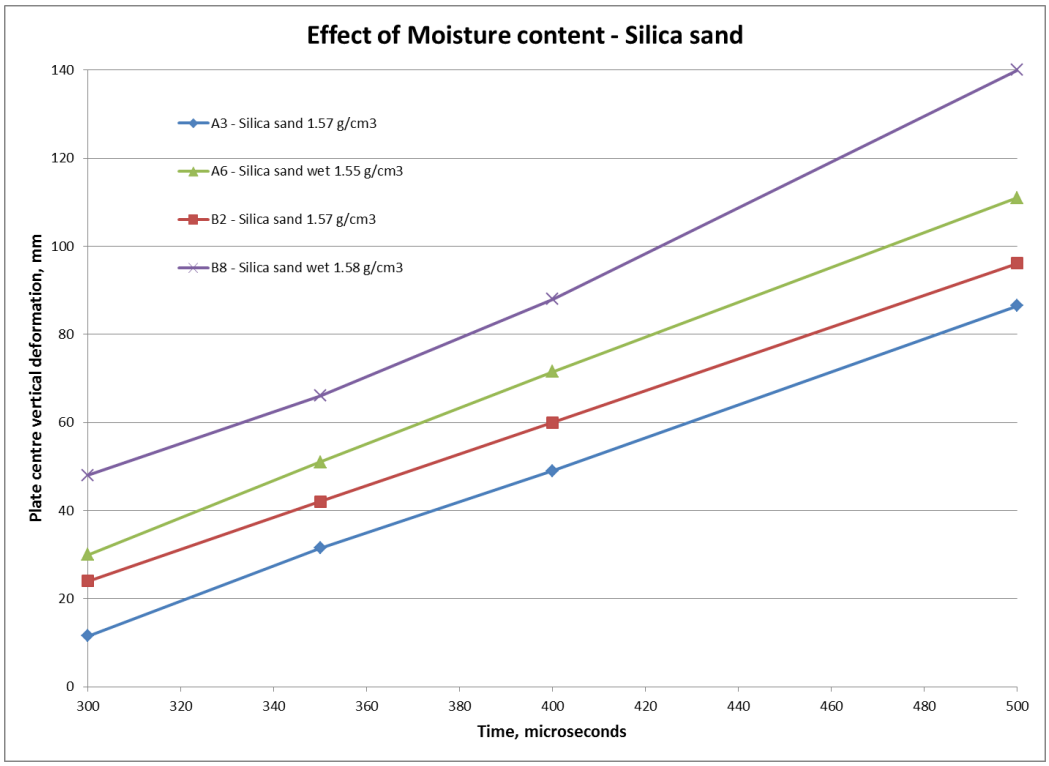

Figure 20 - Plate deformation evolution in time: effect of moisture content (silica sand)

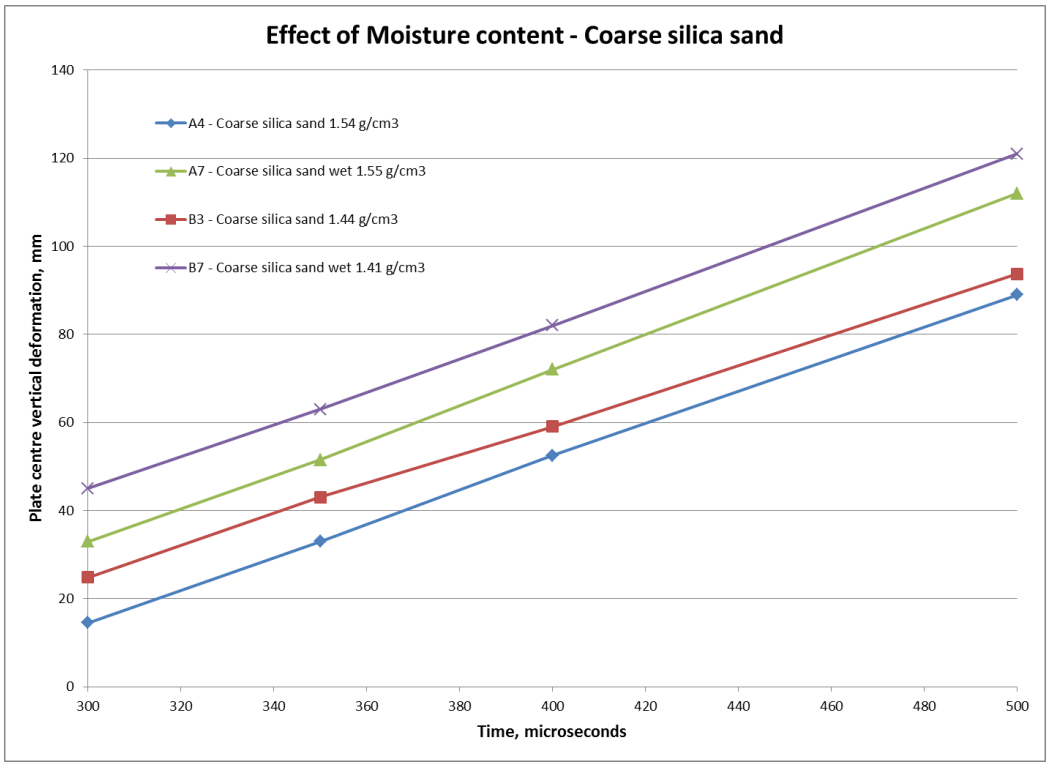

Figure 21 - Plate deformation evolution in time: effect of moisture content (coarse silica sand)

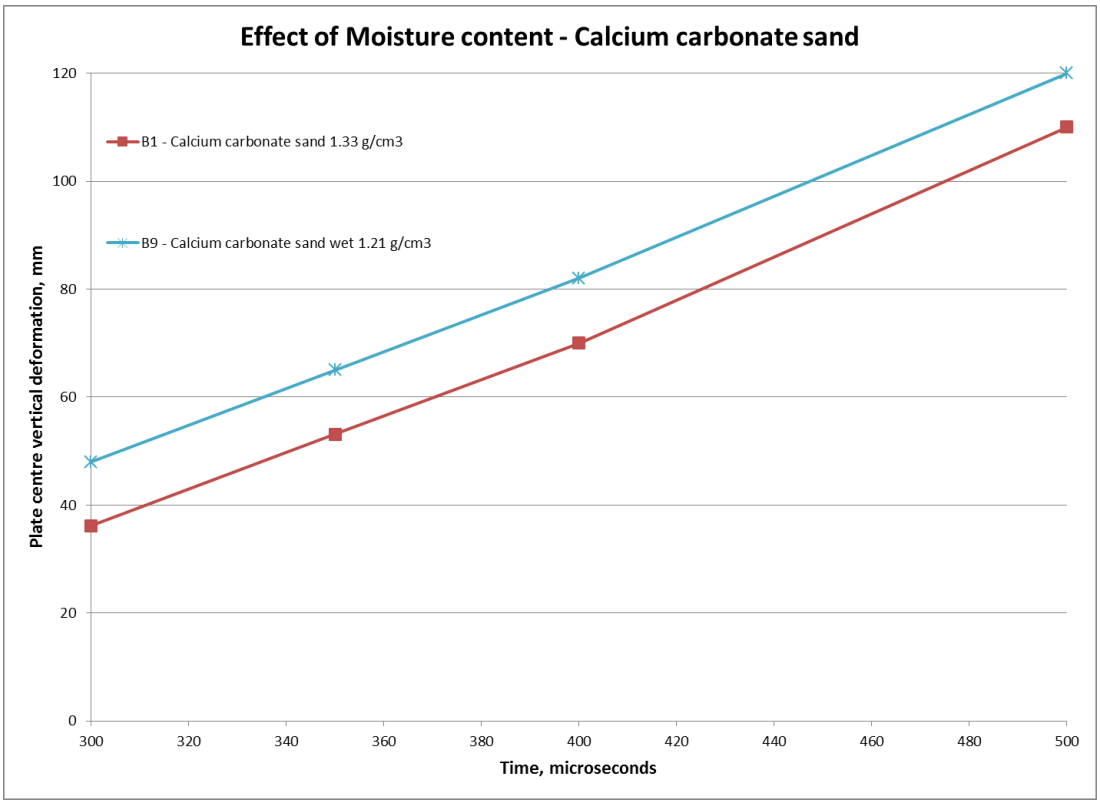

Figure 22 - Plate deformation evolution in time: effect of moisture content (calcium carbonate sand)

The effect of moisture content on the results is shown in Figures 20 – 22 for the silica, coarse silica and calcium carbonate sands, respectively. The results are very consistent, showing an increase in plate deformation at a given time with the inclusion of water, for all the sands tested. This is perhaps the best controlled variable as the material is identical for both tests, only differing in the addition of water. The density was largely matched for both wet and dry tests (except for the calcium carbonate sand), however the implication of this is a different air fraction between the particles which may have some influence on the results. This is evident in the lower measured density for the wet calcium carbonate sand, which can possibly be explained by the sand particles (higher density) being replaced by the water (lower density) rather than the air being replaced by the water and in this case the air fraction value is maintained and closer to that for the corresponding dry test.

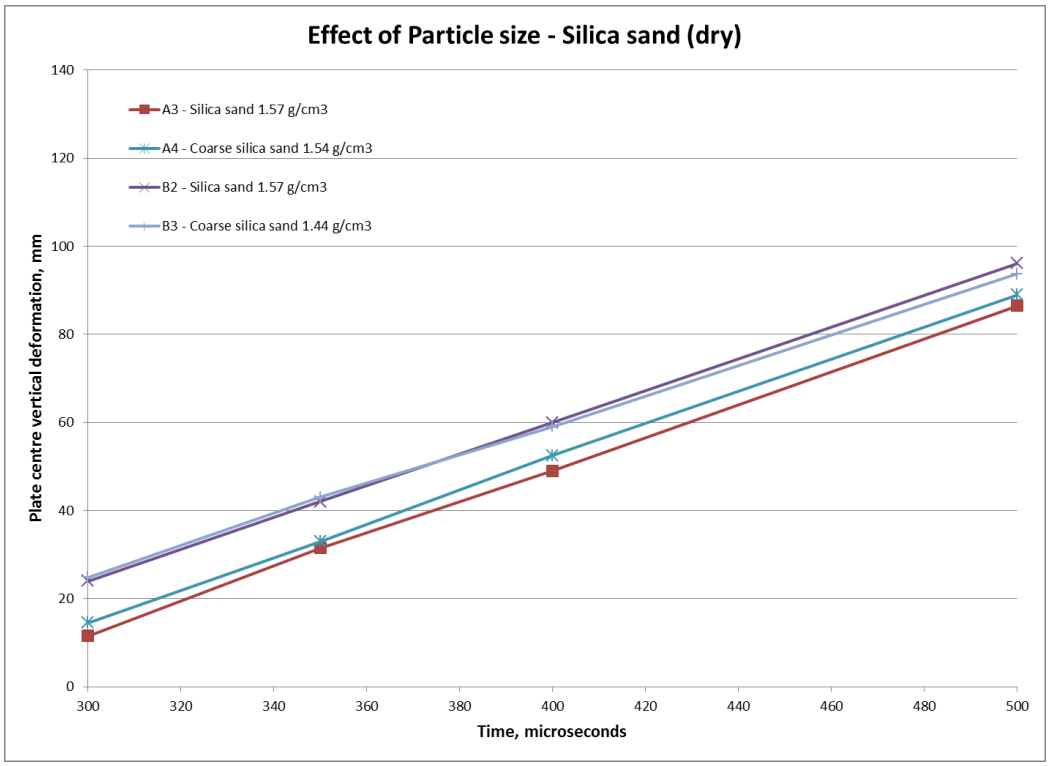

Figure 23 - Plate deformation evolution in time: effect of particle size (dry silica sand)

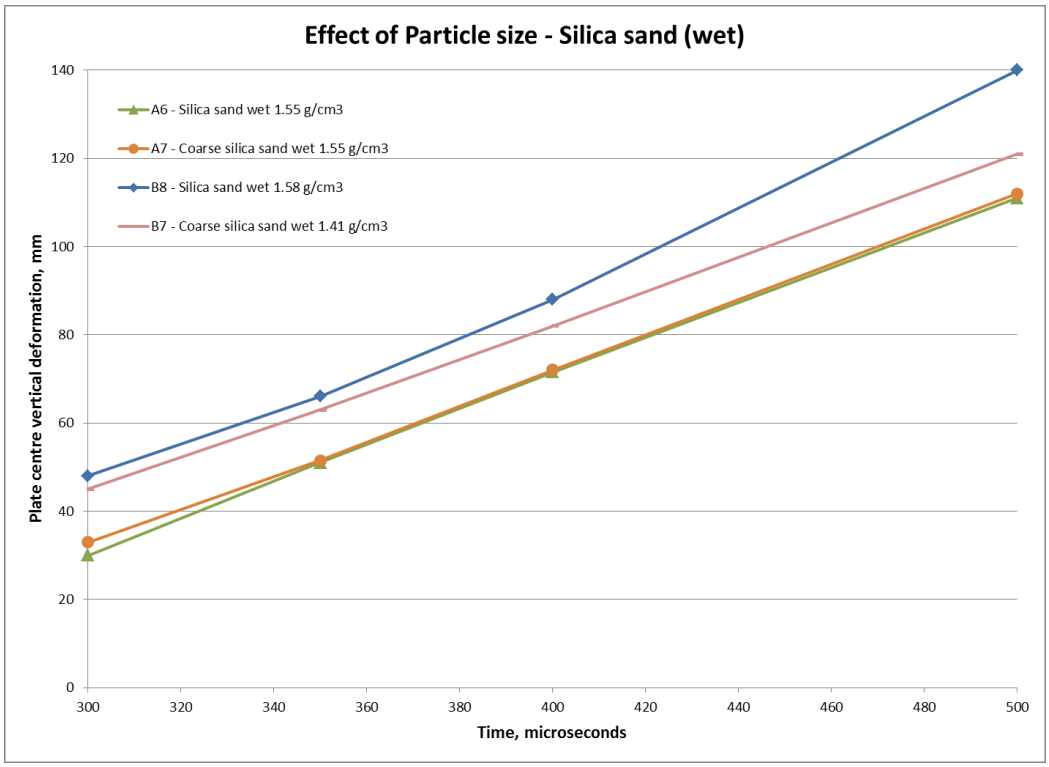

Figure 24 - Plate deformation evolution in time: effect of particle size (wet silica sand)

The effect of particle size on the results is shown in Figure 23 and Figure 24 for the dry and wet silica sands respectively. For the dry silica sand, both the Configuration A tests (A3 and A4) and Configuration B tests (B2 and B3) show that there is only minimal difference in the plate deformation for the fine and coarse silica sands. The densities are matched well for the Configuration A tests, however there is some disparity for the Configuration B tests.

For the wet silica sand, the Configuration A tests (A6 and A7) show a similar result of no difference between the fine and coarse grained silica sands. For the Configuration B tests (B7 and B8), there is some divergence particularly at the later time. It should be noted that here the densities are not very well matched, making the comparison difficult.

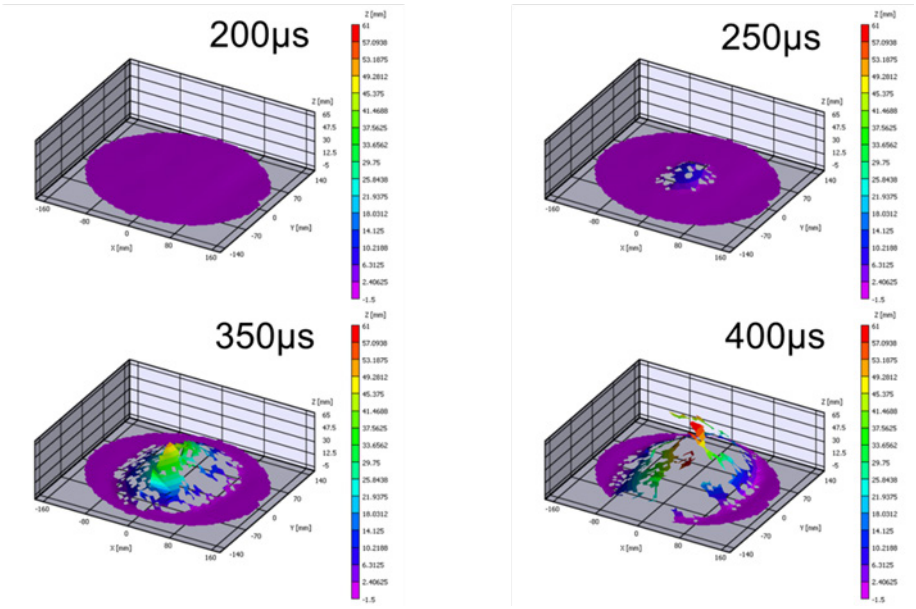

Figure 25 - Digital Image Correlation results

An example of the plate deformation results using the Digital Image Correlation (DIC) technique is shown in Figure 25. The analysis software uses stereoscopic images from two high speed video cameras to calculate the surface strains and deformations of the deforming plate. The cameras were run at 20,000 frames per second (giving a 50 µsec time step), however late in the testing it was discovered that there was an issue with synchronisation of the cameras, resulting in unreliable results. Other limitations of the method for this application include: the inability to position the cameras at the correct angle apart (ideally <60 degrees) due to the fixed position of the explosive chamber viewing ports (~90 degrees); optical distortions through the thick polycarbonate protective viewing ports, necessitating tightly toleranced machined and polished windows and plate deformations limited to the early time only due the arrival of visually obscuring detonation products and ejecta coming around the plate and through after breaching of the target plate. Potentially, with more development, the DIC technique could be used

successfully in this application, however for these tests, the flash x-ray technique was more reliable for measuring the target plate deformation in time.

3.1. Effect of Sand Morphology

The variables assessed in these experiments included sand particle size, particle shape, chemical composition, moisture content and compaction, and their effect on the plate deformation. The most dominant and biggest influence on the output was moisture content, which is well supported by the literature [12]. Particle size and particle shape were seen to have only minimal influence on the plate deformation, whereas, compaction and chemical composition had some influence.

The particle size effect was assessed from the fine and coarse silica sands under both wet and dry conditions. The effect on the plate deformation for these particular materials was minimal and highlights this as an uninfluential variable. However, potentially where sintering may occur in the material, the particle size may play a larger role through its influence on heat transfer and temperature effects due to the importance of length and time scales [13]. In this case, both the fine and coarse silica sands were largely crystalline silica which has a high melting temperature and is not easily sintered under these loading conditions.

The particle shape effect was assessed from the natural angular fine silica sand and the synthetically produced round and spherical soda lime glass beads. The particle shape variable is not completely isolated for this comparison where the chemical composition and material crystallinity also differ between the two materials, however keeping this in mind, there was only a small difference in the results for these two materials. The plate deformation for the glass beads was slightly higher. The spherical shape of the glass beads means that they only have essentially one packing density. They cannot be reorientated to compact further and thus the overall material stiffness/compressibility is relatively high from the onset of compaction. The angular shaped particles of the silica sand however can undergo an initial stage of particle reorientation under an applied compressive load, increasing the packing density and resulting in a low stiffness, high compressibility in the initial stages of loading. In addition, the inter-particle interactions are different in each case, specifically the inter-particle friction and mechanical forces are expected to be higher in the angular particle case. This is potentially important once the loads get higher and particle crushing starts to occur.

The stiffness of the bulk material is also an important concept when considering the effect of moisture content, which was seen to be the most influential variable on the results. Increasing the moisture content in the sand, results in a significantly higher plate deformation at a given time. This was seen consistently for the fine silica sand, coarse silica sand and calcium carbonate sand. In all cases the addition of 10% moisture content resulted in a similar increase in the plate deformation. The overall material bulk density was kept constant for the dry and wet sands, hence isolating the moisture content variable. The inclusion of water displaces some of the air between the particles and makes the overall material response stiffer and less compressible. This provides better coupling with

the target plate for greater momentum transfer. This is a somewhat simplistic view, and in reality there are more complex mechanisms at play, including but not limited to: possible lubrication effects between particles, phase changes within the water, inter-phase interactions and thermal and dissipative effects between the air, water and solid particles [9].

The effect of the sand chemical composition was assessed from the calcium carbonate and silica based sands, where in each case these were primarily crystalline materials. The effect of crystallinity was also assessed for the silica where crystalline silica sand was compared to soda-lime glass (silica based) amorphous glass beads, however in this case the variable was not completely isolated as the particle shape was not constant and there was also some variation in the chemical composition. One of the important aspects related to the chemical composition and material crystallinity appears to be the melting point of the material, which can influence potential sintering between the particles under the high pressure and temperature explosive loading. In a general sense, increasing crystallinity will increase the melting point and make sintering less likely (crystalline silica has a much higher melting point compared with amorphous silica glass) and the sintering is associated with the strength of the sand body. The chemical composition or mineralogy of the sand obviously affects the melting temperature (calcium carbonate has a lower melting point than silica), and impurities within the material can also have a large effect on the melting point.

The effect of compaction was assessed with the calcium carbonate sand which was tested loosely packed and in a tamped condition, giving a difference in bulk density of approximately 10-15%. Additionally, for the Configuration B series of tests, a very high porosity silica based material, diatomaceous earth, with a bulk density of only 0.14g/cm^3 was tested to investigate the effect with a low bulk density material which has a large air phase. For the calcium carbonate sand, the compacted state gave less deformation at the plate centre at a given time compared with the loosely packed sand. However, the centre plate deformation is only one aspect of the plate deformation response. The shape of the deformation is also very important for overall how much momentum is imparted to the plate. CTH numerical modelling of the setup shows that with decreasing bulk density of the sand material, the shape of the plate deformation changes from bell shaped at high density to a nipple shape, more localised in the centre as the density decreases. This change in plate deformation shape is in direct response to a change in shape of the ejecta which is providing the loading and specifically and probably more importantly the mass and velocity distribution within that ejecta which is not captured by the flash x-ray but does manifest itself in the plate deformation profile.

An additional reason for the compacted response is the ejection process occurs slower with lower velocity due to the increase in mass, and so it takes longer for ejecta to be accelerated up to the plate. This is highlighted very well in the case of the low bulk density diatomaceous earth, which has less mass so it gets accelerated quickly. The flash x-ray timings for this material were much earlier than for all the other materials tested, with the onset of plate deformation occurring prior to 100 μsec.

Finally, the effect of compaction and the material bulk density is also highly influenced by the experimental setup used. Specifically, the reflective steel base of the container means there is no energy dissipation below the charge. This is a critical difference compared to having the charge buried in an infinite sand medium. In the latter, energy will be dissipated below the charge and for a low density material the energy directed downwards is lost. As the material bulk density increases and if the charge burial is shallow, the high density material underneath helps to reflect some of the energy upwards. However, in the experimental setup used here all of the downward energy is reflected upwards by the steel base for both and low and high density materials.

The charge initiation configuration also had an effect on the loading to the sand and subsequent deformation of the target plate. While this wasn't a specific variable within the sand, it exposed the different sand materials to two different loading conditions. Configuration A was point initiated at the centre of the base of the charge, whereas Configuration B was simultaneously initiated over the base area of the charge. The Configuration B initiation was achieved using an explosive plane wave generator, which consisted of two different speed explosives to tailor the shape of detonation wave to produce a 1D planar detonation wave. The main charge was the same for both configurations, however the explosive plane wave generator had the effect of adding additional explosive for Configuration B. The two configurations produce different spatial distributions of the loading to the sand and this was subsequently seen in the deformation of the target plate, specifically the shape of the deformation. The plane wave initiated charge of Configuration B produces a more focussed/ directed loading above the charge resulting in less width to the target plate deformation, whereas the point initiated Configuration A produces a more spatially distributed loading which is subsequently seen as a broader plate deformation profile. The Configuration B tests consistently produced a higher centre plate deformation for this reason and also due to the higher explosive content.

4. Numerical Analysis

A numerical analysis of the setup has been conducted for one of the sands tested, namely the dry, uncompacted calcium carbonate (calcite) sand, corresponding to the experimental tests A8 and B1 for the two different charge configurations. The numerical simulation employs a two-phase material model for the sand which had been applied in previous work [6] to the quasi-2D setup involving a rectangular target plate. The current simulations of the cylindrical 2D axisymmetric setup are limited to the same dry, uncompacted calcium carbonate sand used previously in order to compare the influence of the old and new setups, where the current setup eliminates the three-dimensional influence observed previously. The current simulations employ the same parameters for the sand material used previously, with slight variations in density which is taken as ρ_0 = 1.31 g/cm^3 for the test employing the Configuration A charge and ρ_0 = 1.33 g/cm^3 for the Configuration B charge.

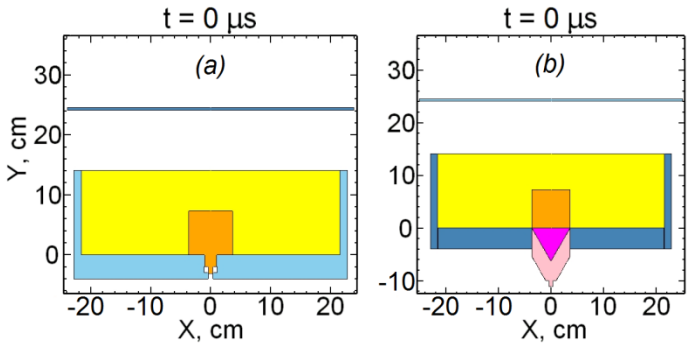

Figure 26 – Numerical schematic set-ups for the Configuration A charge (a) and the Configuration B charge (b)

Numerical schematics of the present set-ups for the charge configurations A and B are shown in Figure 26. The yellow area represents the sand material, the blue area is the steel casing and aluminium target plate at the stand-off distance of 10 cm, and the orange area represents the main explosive charge, which has a small extra area (booster) for initiating detonation (Figure 26 (a)) and pink and magenta areas for the plane wave generator representing different explosives (Figure 26 (b)) for the Configuration B charge initiation.

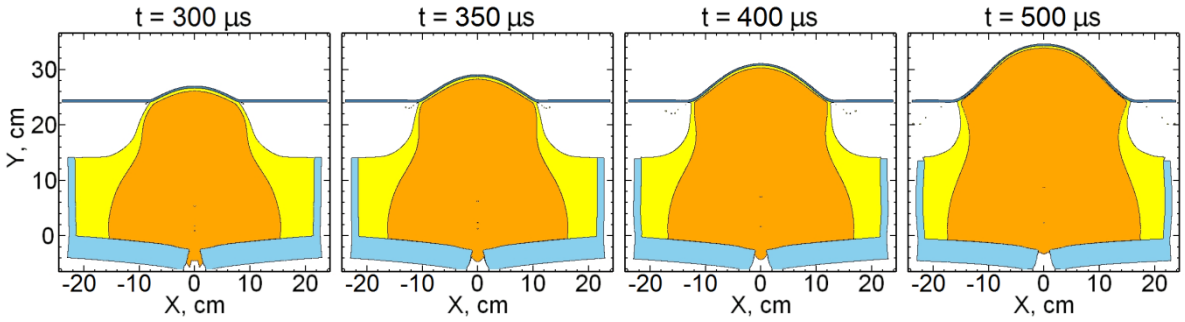

Figure 27 – CTH two-phase simulation of the plate deformation due to the sand ejecta impact from the Configuration A charge at t = 300, 350, 400, and 500 µs after initiation

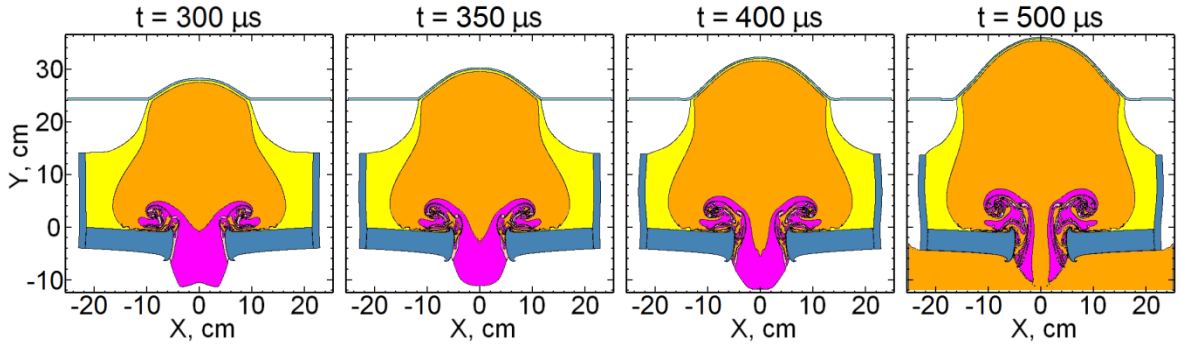

Figure 28 – CTH two-phase simulation of the plate deformation due to the sand ejecta impact from the Configuration B charge at t = 300, 350, 400, and 500 µs after initiation

The results of the CTH numerical simulations for the Configuration A and B charges are shown in Figure 27 and Figure 28, respectively, where the two-phase material model is employed for the sand. It can be seen that the Configuration B charge provides a slightly higher momentum transfer to the target plate that is in agreement with the experimental observations.

Referring to the previous analysis conducted for the rectangular setup in [6], the CTH simulations employing a simpler Sesame tabular EOS description for the sand material resulted in a slightly larger momentum transfer to the target plate compared with the two-phase description of the sand. A yield limit of Y = 10 MPa was used together with the Sesame EOS in the simulations [6], which seems to be an overestimate for the real material even in a consolidated state, however, this value enables a reasonable correlation with the experiments [6].

In order to conduct a similar comparison for the present 2D axisymmetric set-up, the same 'Dry Sand' Sesame tabular EOS with the P-α model [7] was utilized as in the previous calculations and yield limit of Y = 10 MPa. The initial densities of the sand are selected as for the two-phase calculations above (Figure 27 and Figure 28).

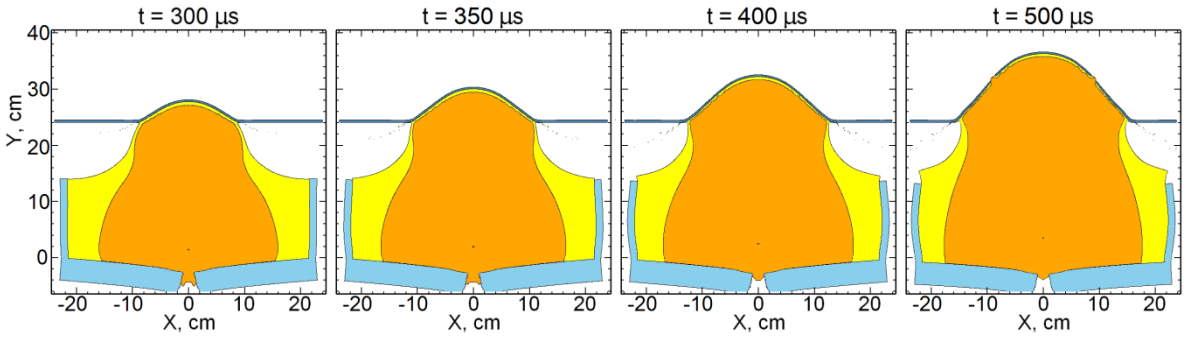

Figure 29 – CTH Sesame EOS simulation of the plate deformation due to the sand ejecta impact from the Configuration A charge at t = 300, 350, 400, and 500 μs after initiation

The numerical simulation results employing the 'Dry Sand' Sesame EOS with P-α model for the present set-ups are shown in Figure 29 and Figure 30 for the Configuration A and B charges, respectively.

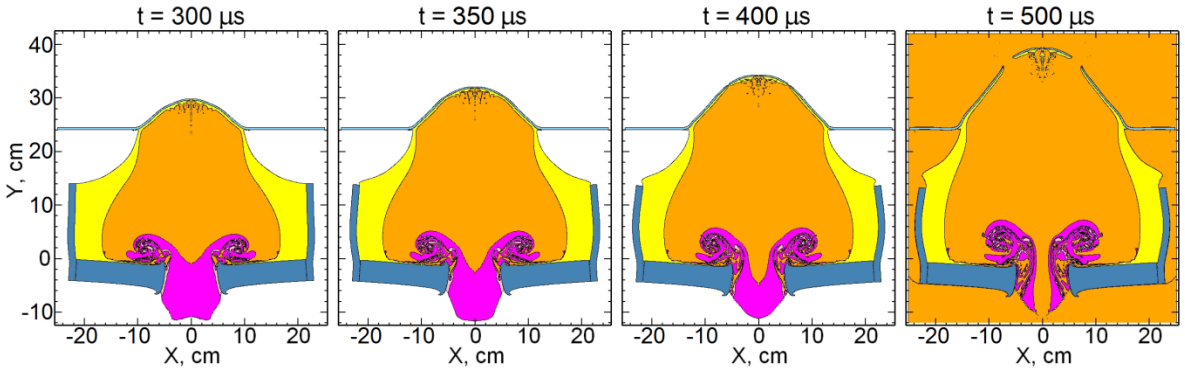

Figure 30 – CTH Sesame EOS simulation of the plate deformation due to the sand ejecta impact from the Configuration B charge at t = 300, 350, 400, and 500 µs after initiation

From these simulations, the same trend of a higher momentum transfer to the target plate is observed when employing the Sesame 'Dry Sand' tabular EOS model compared with the two-phase model for the sand. In order to evaluate the accuracy of the calculations and compare which sand model describes the momentum transfer better, the calculation results need to be compared with the experiments.

The corresponding experiments are represented by Event A8 for the Configuration A tests, and by Event B1 for the Configuration B tests as seen from the test summary in Appendix A.

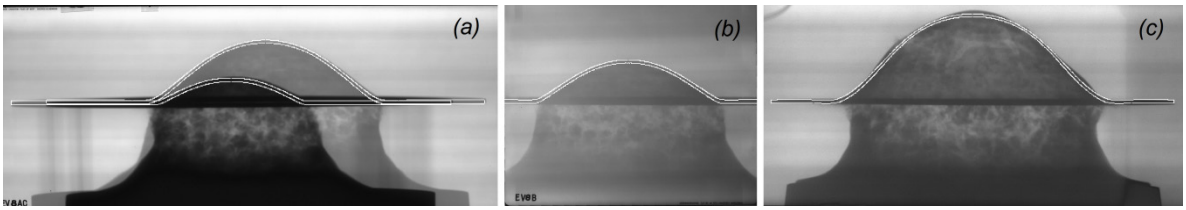

Figure 31 – Comparison of the two-phase CTH calculation for the Configuration A charge with experiment A8 at t = 300, 400 (a); 350 (b); and 500 µs (c)

A comparison of the results of the CTH calculation employing the two-phase model for the sand for charge Configurations A and B are shown in Figure 31 and Figure 32, respectively. The calculation results are limited only to the images of the target plate contours (white contours) superimposed with the flash x-ray experimental images for the respective tests.

The results demonstrate an excellent agreement, which is remarkable in view that the parameters of the two-phase model were fitted from independent experiments (see [10-11]) and previously validated with an independent set of tests [6].

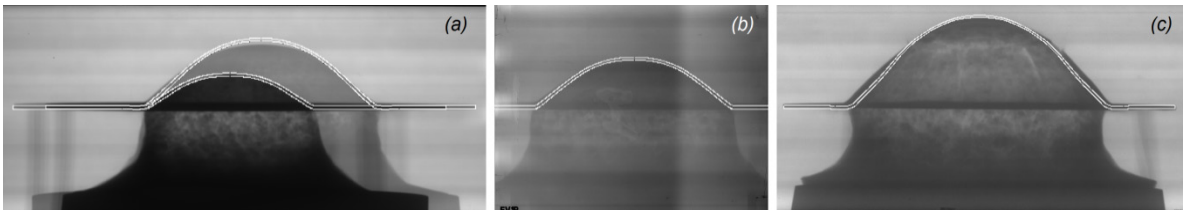

Figure 32 – Comparison of the two-phase CTH calculation for the Configuration B charge with experiment B1 at t = 300, 400 (a); 350 (b); and 500 μs (c)

For completeness, we also compared the numerical results employing the Sesame 'Dry Sand' tabular EOS from the CTH material database, that are shown in Figure 29 and Figure 30, with the same tests.

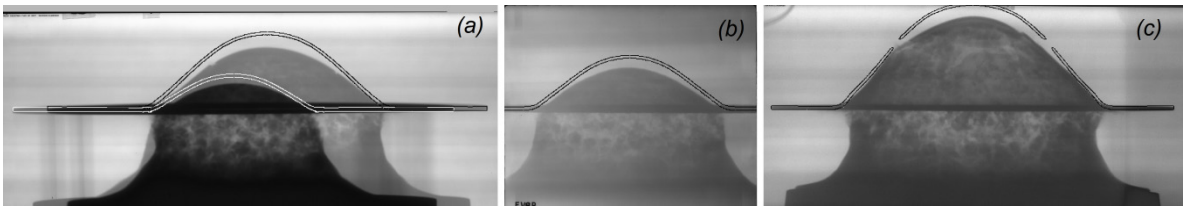

Figure 33 – Comparison of the Sesame EOS CTH calculation for the Configuration A charge with experiment A8 at t = 300, 400 (a); 350 (b); and 500 μs (c)

The comparison is shown in Figure 33 and Figure 34 for the Configuration A and B charges, respectively.

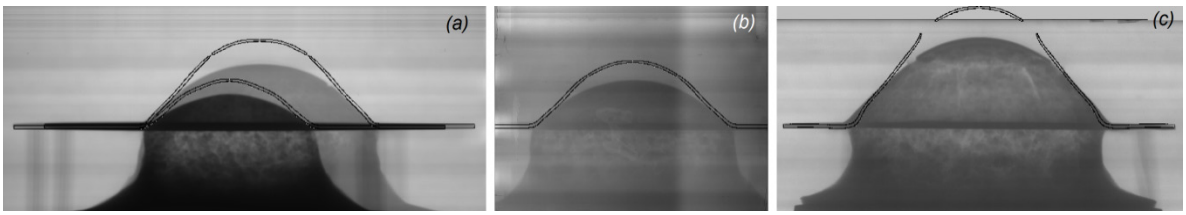

Figure 34 – Comparison of the Sesame EOS CTH calculation for the Configuration B charge with experiment B1 at t = 300, 400 (a); 350 (b); and 500 μs (c)

It is clearly seen that the plate deformation is excessive for the calculations using the Sesame 'Dry Sand' tabular EOS, indicating an excessive momentum transfer to the target. This disagreement is moderate for the Configuration A charge (Figure 33) and worse for the Configuration B charge (Figure 34), where the shock dissipation is larger in the vertical direction compared to the more isentropic loading of Configuration A. Specifically, the shock dissipation description is worse with the P-α model used with the Sesame 'DrySand' tabular EOS, as this model significantly underestimates the Hugoniot temperature [14].

5. Analysis

The previous experimental setup, involving a rectangular target plate, reported in [6] had the disadvantage of only being quasi-2D which made it difficult to compare to 2D simulations and necessitated approximations relating to the third dimension. This included multidimensional effects which potentially influenced the calculation results such the escape of detonation products in the lateral directions in the later stages of the target plate loading. The present experimental setup avoids these deficiencies by using a cylindrical axisymmetric arrangement which can be simulated numerically in 2D without assumptions and analysis of the 3D geometry influence. Thus the axisymmetric experimental setup made it amenable to comparison with two-dimensional simulations where the two charge variants (Configuration A and B) were analysed numerically for the case of the dry, uncompacted calcium carbonate sand used previously in [6].

The constitutive equation fitted in [6] is only suitable for dry calcium carbonate (calcite) sand. However, similar fitting of constitutive equations is possible for the other sands analysed in this report, specifically using the methodology developed and detailed in [6]. The methodology involves using Split Hopkinson Pressure Bar (SHPB) data for fitting strength constitutive equations and a compaction kinetic, followed by validation of the model as conducted here for the case of dry calcite sand.

In the course of a previous analysis [8] one might believe that a conventional material model from the CTH material model database could be used for the analysis, because the momentum output for the corresponding calculation was in reasonable proximity (within 10%) to the experimental observations, even though not as accurate as the calculation with the two-phase material model [9] implemented in CTH. However, the divergence seems to be more obvious for the calculations involving the plate deformation response [6]. The present analysis shows that this divergence is not of the occasional nature and is confirmed with the present axisymmetric setup calculations also.

The extended set of sand/soil materials investigated with the present experiments allowed for an evaluation of some of the material parameters of the sand on the loading and subsequent momentum transfer to the target plate. The material morphology did not demonstrate a significant influence of the results. This is evidenced by comparing the silica sand and glass beads response in Figure 17 for both the Configuration A tests (Events A3 and A5) and the Configuration B tests (Events B2 and B5), whereby the plate deformations with time are fairly similar for the two materials with different particle shape. However, a lubrication effect from moisture content in combination with particle shape was not assessed in these experiments, where there was some evidence of an effect seen with moisture content in combination with different particle sizes. This is evidenced by comparing the wet coarse silica sand and wet silica sand response in Figure 14 for the Configuration B tests (Events B7 and B8), where the curves are relatively close for the first half of the observed plate deformation but increases significantly for the finer sand at the second half. It should be noted that the average densities for these two cases are notably different, however this may not provide an argument because of the closeness of the curves for the first half of the plate deformation. Without the moisture content

contribution, the particle size effect was minimal as evidenced in Figure 23 for the equivalent dry fine and coarse silica sands.

In general, the density of the sand had the effect of a trend towards a larger plate deformation for a less dense medium. This is shown for the uncompacted and compacted calcium carbonate sand in Figure 12 for both the Configuration A tests (Events A8 and A2) and the Configuration B tests (Events B1 and B4). However, the most striking example relates to that for the very low density diatomaceous earth material (Event B6) in Figure 11. Here the very light material is accelerated quickly and reaches the target plate earlier. However, the graphs only present the plate deformation at the centre, where the shape of the deformation is also quite different being more localised towards the centre for the low density material. Referring back to Figure 12, there is a significant increase in plate deformation for the lightest wet sand amongst the calcium carbonate sand tests. However, the lower density is not the main reason for the displacement increase but rather the strong influence of the water content, which might be associated with the phase transition of the interstitial water to vapour. This moisture effect was seen in all the investigated media, where the deformation increase with the inclusion of water is seen in Figure 20 and Figure 21 for the silica and coarse silica sands also, and highlights the strong influence of the water content on the loading.

Quite expectedly, the plate displacement was consistently larger for the tests with the Configuration B charge compared with the corresponding Configuration A charge tests, somewhat due to the additional explosive mass. However, the planar initiation for the Configuration B charge also results in a focussing of the explosive products in the vertical direction, compared with the point initiated Configuration A charge which has more energy distribution laterally. The increased displacement was seen consistently for the calcium carbonate sand tests in Figure 12, the silica sand tests in Figure 13, the coarse silica sand tests in Figure 14 and the glass beads tests in Figure 15.

The effect of the type of sand, or its chemical composition, is presented in Figure 19 comparing the calcium carbonate and silica based sands. The comparison is difficult to make because the calcium carbonate sand, even in its pre-compacted state is typically less dense than the silica sand. However, the factor of composition cannot be neglected as seen in Figure 11 when comparing the plate centre displacement for the wet roadbase material (Event B10) with the corresponding curves for the wet sands of Events B7, B8 and B9. As expected for the less dense sands the displacement is larger, although the rate of increase for the roadbase material is notably larger and almost reaching the wet sand curve for Event B7 at the event of the observation period.

The rate of change for the displacement curve approximately corresponds to the average plate velocity. Typically, as can be assessed from Configuration A tests in Figure 10, the average plate velocity is close to 400 m/s and approximately 350 m/s for the sands with conventional density for the Configuration B tests in Figure 11. However, the extremity in density for the diatomaceous earth, possibly resulting in the Hugioniot abnormality for highly porous materials, sees the velocity increase up to almost 1000 m/s and the extremity in the chemical composition for the roadbase soil, possibly resulting in material

consolidation and crushing of large aggregate components, sees the velocity increase up to approximately 450 m/s for the Configuration B tests.

Observing the shape of the target plate deformation, it should be noted that when deviating from the median material density range of 1.3-1.6 g/cm^3, there is an accompanying change from the standard inverted U-type shape to a bell shape with a higher load localisation at the centre of the plate for a low density medium to a more shallow shape with a wider load distribution for a high density medium. This can be seen in the flash x-ray images in Appendix A, particularly for the diatomaceous earth (Event B6) as a low density material and the wet roadbase (Event B10) as a high density material.

6. Conclusion

An experimental setup, which takes advantage of an axisymmetric cylindrical configuration that can be simulated numerically in two-dimensions, has been developed and used for assessing the loading on a target plate from a buried explosive charge for a variety of sands and a soil. The target plate deformation, as a measure of momentum transfer to the plate, is determined using the flash x-ray technique and the influence of the sand parameters on the loading and plate deformation have been investigated and discussed.

The density of the sand/soil media is identified as the most critical parameter in the response, followed by the water content in the material. At the same time, while not being immediately obvious, the influence of the material morphology (particle shape and size) and chemical composition may also be important.

Constitutive equations of the two-phase model [9] for dry calcium carbonate (calcite) sand, obtained with the experimental methodology developed and detailed in report [6], have proved their fidelity for correctly describing the sand response when comparing the calculation results with the experiments as a validation data set.

The calculations utilizing the same models [6] with the present experimental setup demonstrates that the poorer description obtained using a conventional tabular EOS model for the sand when compared with the proposed two-phase model, is even more profound with the current experimental setup. Therefore, this deficiency is likely to be driven by an inadequate physical description of the material, with this gap covered by the present two-phase model as shown with the present calculations and comparisons with the experiments.

7. Acknowledgements

The authors would like to thank the technical staff from the High Explosive Firing Complex (HEFC) facility for facilitating these tests, namely Trevor Delaney as firing officer; Steven Stojko and Jared Freundt for instrumentation support; Mark Rausch and Stewart Kennedy for the flash X-Ray instrumentation; and Mark Mitchell for manufacture of the explosive charges.

8. References

1. Fourney W.L., Leiste U., Bonenberger R., and Goodings D., Explosive impulse on plates, Fragblast, 2005, v. 9, n. 1, pp. 1-17.
2. Anderson C.E. Jr, Behner T., and Weiss C.E., Mine blast loading experiments, Int J. Impact. Eng., 2011, v. 38, pp. 697-706.
3. Bergeron D.M. and Tremblay J.E., Canadian research to characterise mine blast output, 2000, In: 16th Int MABS Symp, Oxford, UK, p 5
4. Bergeron D., Walker R., and Coffey C., Detonation of 100-gram anti-personnel mine surrogate charges in sand e a test case for computer code validation, Technical Report DRES-SR-668, 1998, Defence Research Establishment Suffield, Canada.
5. Hansen C. and Pak R.Y.S., Centrifuge characterization of buried, explosive-induced soil ejecta kinematics and crater morphology, J. Dyn. Behav. Mater., 2016, v. 2, n. 3, pp. 306-325.
6. Resnyansky A.D., Weckert S.A., and Rausch M., Study of Dynamic Momentum Transfer to a Target Loaded by a Buried Charge, Technical Report, DST-Group-TR-3448, 2018, Defence Science and Technology Group, Australia.
7. Bell R.L., Baer M.R., Brannon R.M., Crawford D.A., Elrick M.G., Hertel E.S. Jr., Schmitt R.G., Silling S.A., and Taylor P.A., "CTH user's manual and input instructions version 7.1", 2006, Sandia National Laboratories, Albuquerque, NM.
8. Resnyansky A.D., CTH Implementation of a Two-Phase Material Model With Strength: Application to Porous Materials, Technical Report, DSTO-TR-2728, 2012, Defence Science and Technology Organisation, Australia.
9. Resnyansky A.D., Constitutive modeling of shock response of phase-transforming and porous materials with strength, J. Appl. Phys., 2010, v. 108, n. 8, pp. 083534-13
10. Weckert S.A. and Resnyansky A.D., Use of SHPB tests for incorporating a compaction constitutive equation within a two-phase model, AIP Conf Proc, 2018, v. 1979, pp. 110019.
11. Weckert S.A. and Resnyansky A.D., Deformation and Shock Consolidation of Various Sands under Explosive Loading, AIP Conf Proc, 2017, v. 1793, pp. 120013.
12. Omidvar M., Iskander M., and Bless S. Stress-strain behavior of sand at high strain rates, Int. J. Impact Eng., 2012, v. 49, pp. 192-213.
13. German R.M., Sintering theory and practice, 1996, John Wiley & Sons, New York.
14. Resnyansky A.D. and Weckert S.A., Experiments and Constitutive Modelling of Sand Ejecta Impact, J. Dynamic Behavior of Materials, 2018, v. 4, n. 4, pp 586–607.

Appendix A – Plate Deformation Profiles

A.1. Charge Configuration A Tests

Event A2 – Calcium carbonate sand, dry, compacted, ρ=1.49 g/cm³

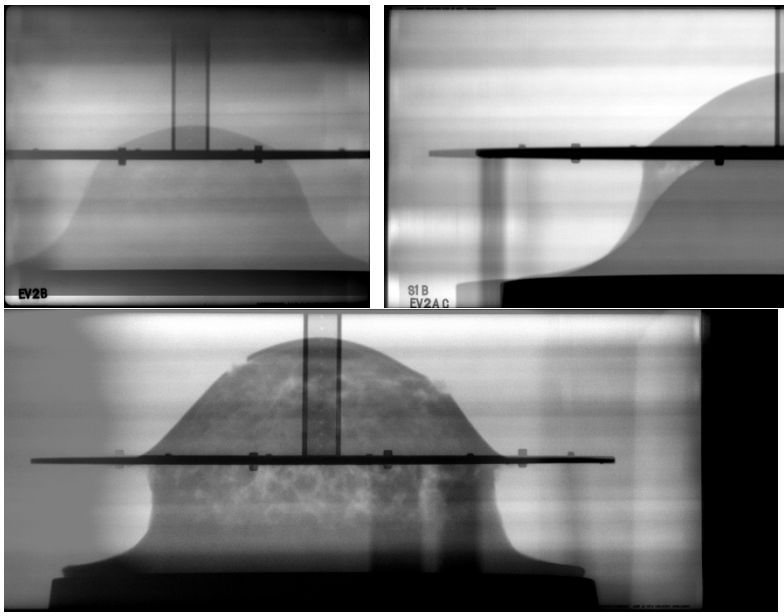

Event A3 – Silica sand, dry, ρ=1.57 g/cm³

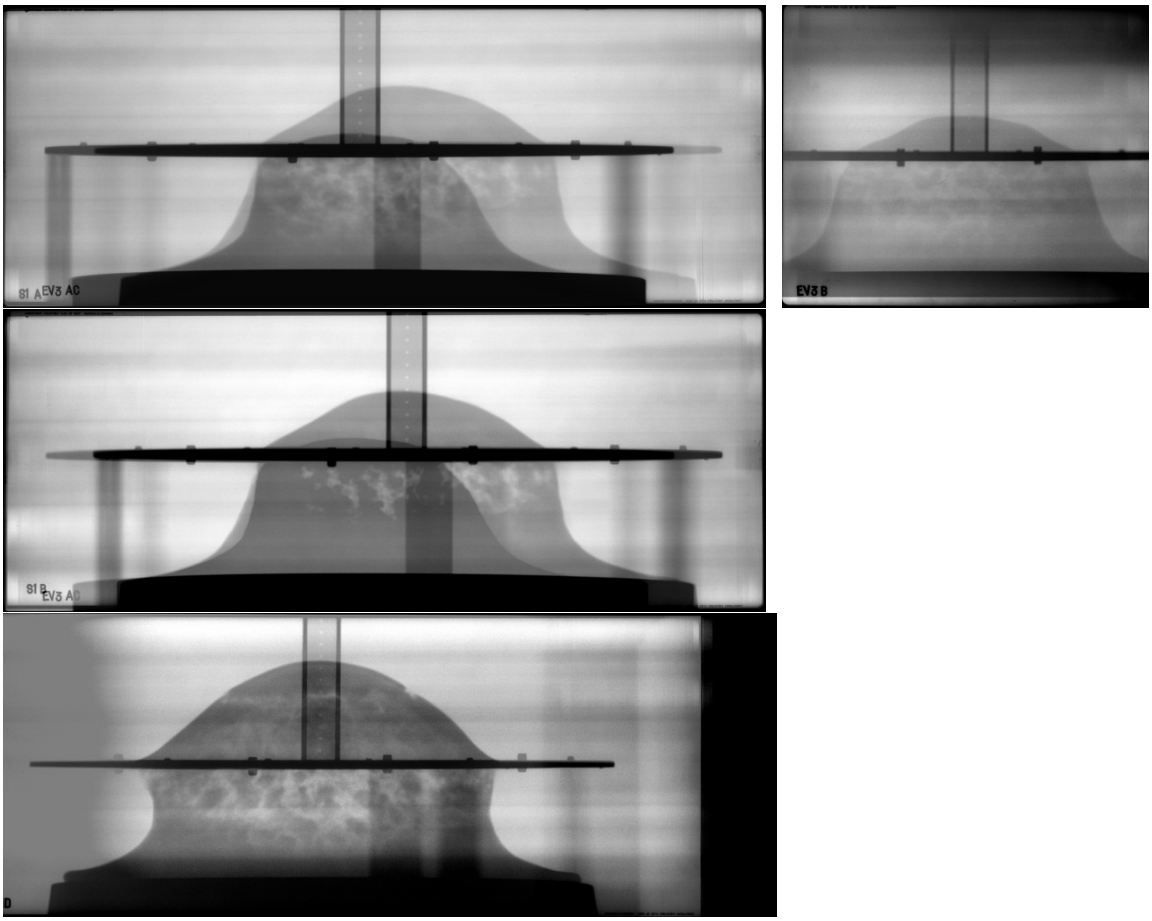

Event A4 – Coarse silica sand, dry, ρ=1.54 g/cm³

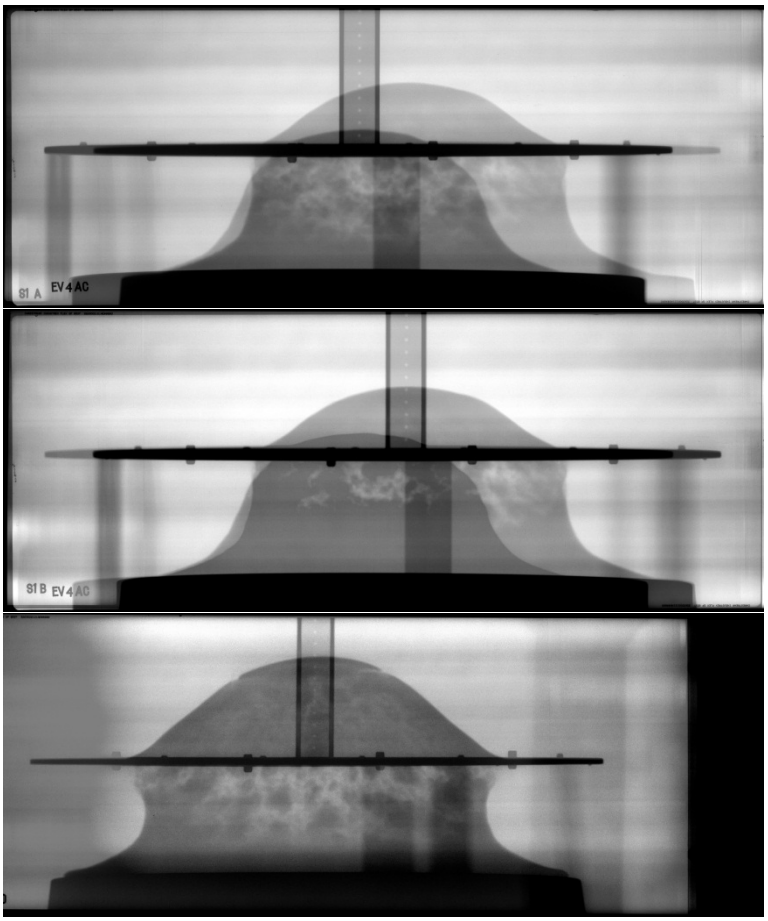

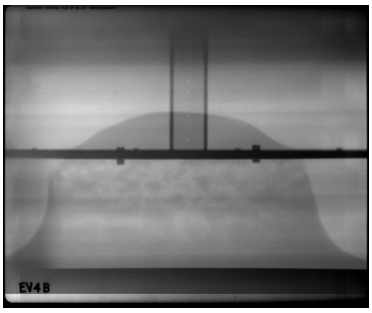

Event A5 – Glass beads, dry, ρ=1.54 g/cm³

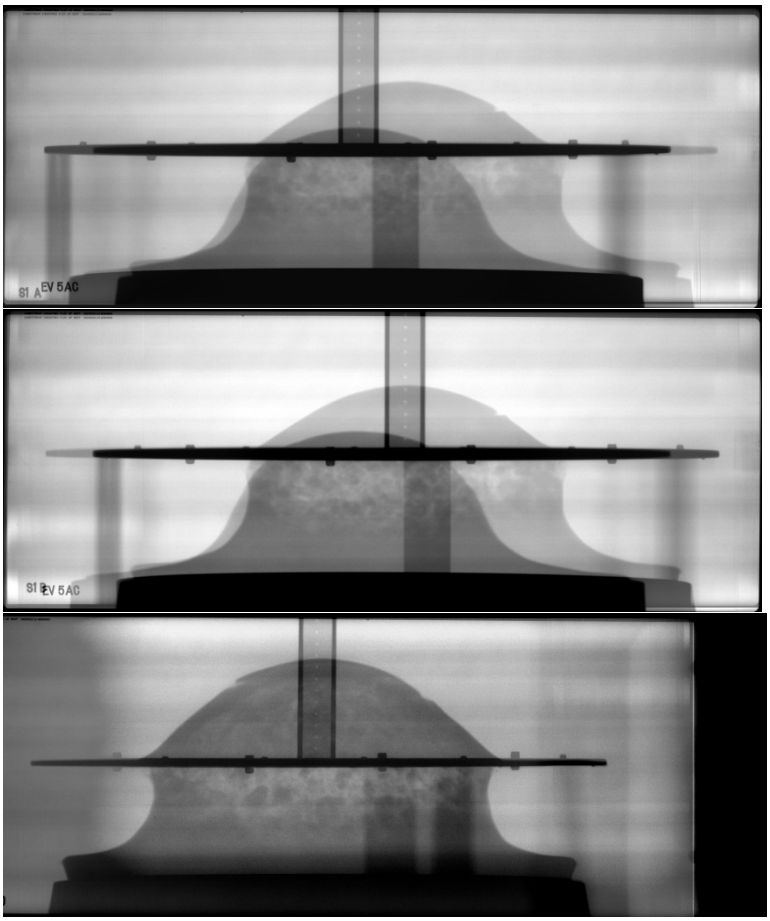

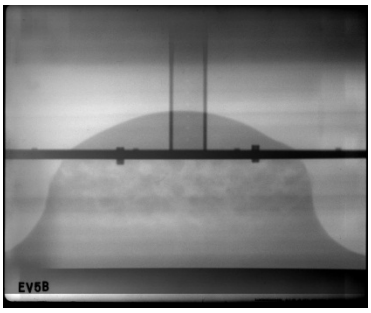

Event A6 – Silica sand, 10% moisture, ρ=1.59 g/cm³

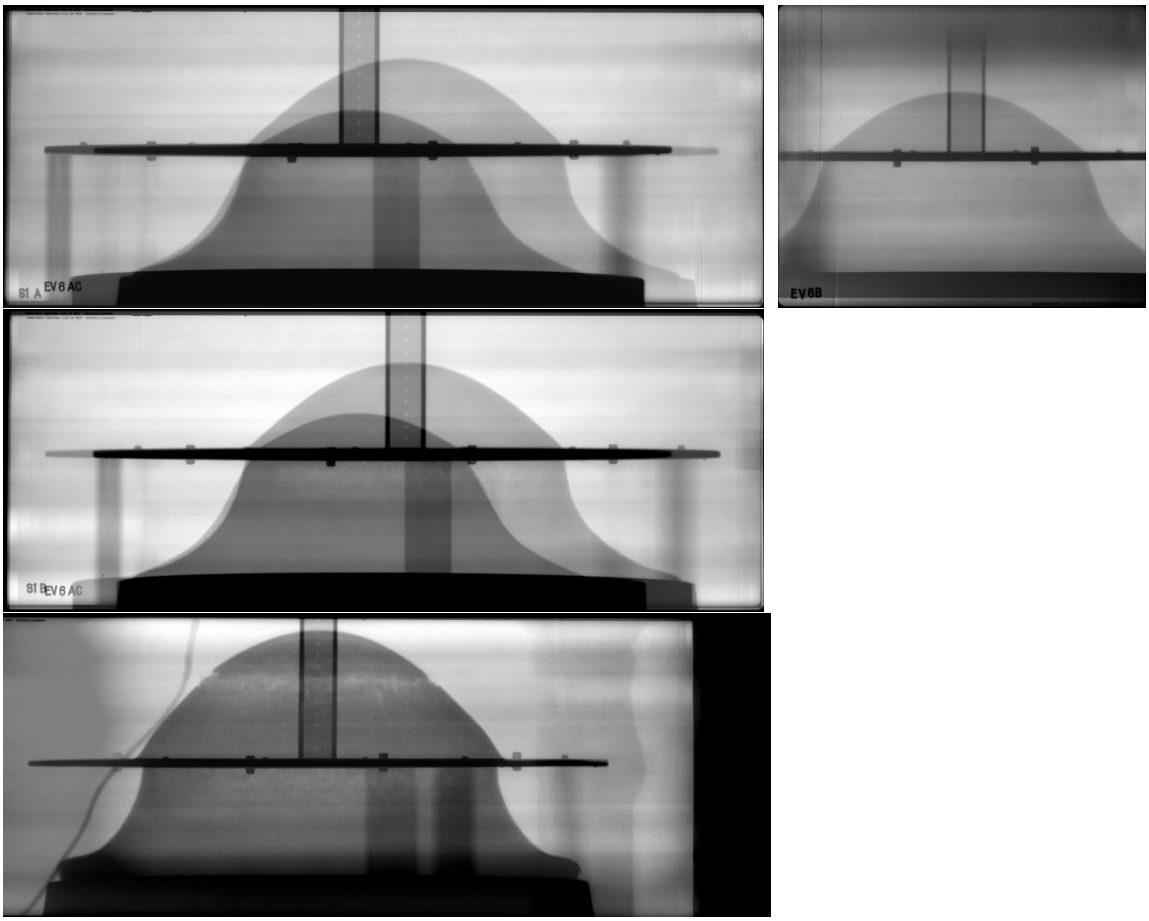

Event A7 – Coarse silica sand, 10% moisture, ρ=1.55 g/cm³

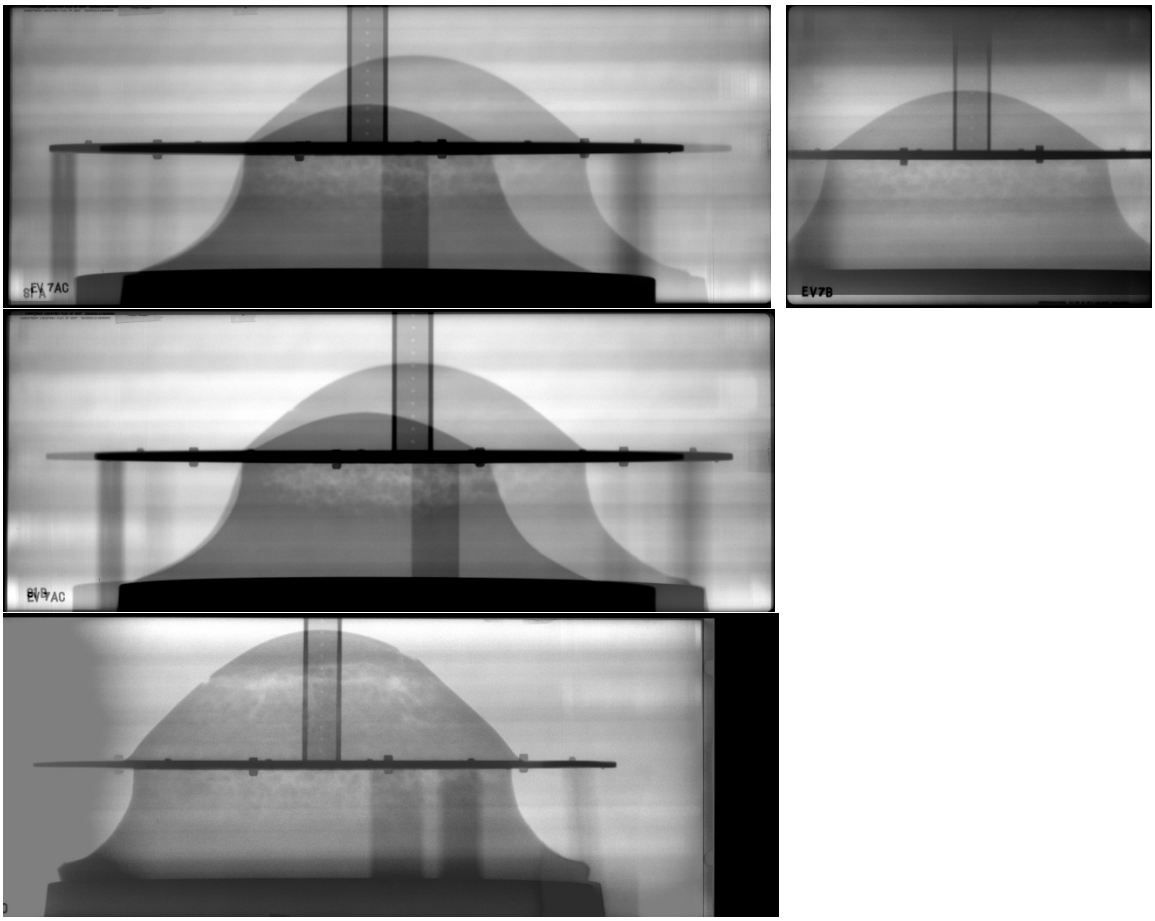

Event A8 – Calcium carbonate sand, dry, uncompacted, ρ=1.31 g/cm³

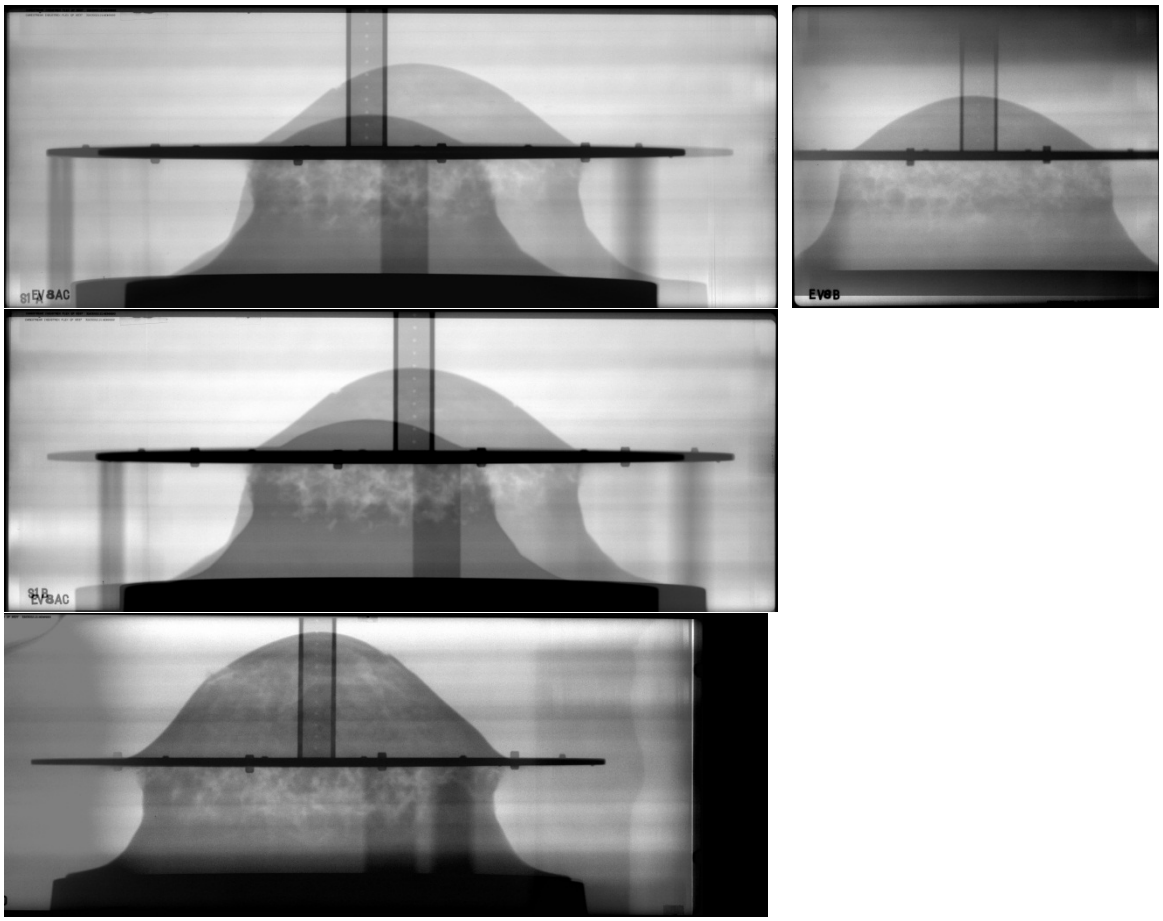

A.2. Charge Configuration B Tests

Event B1 – Calcium carbonate sand, dry, ρ=1.33 g/cm³

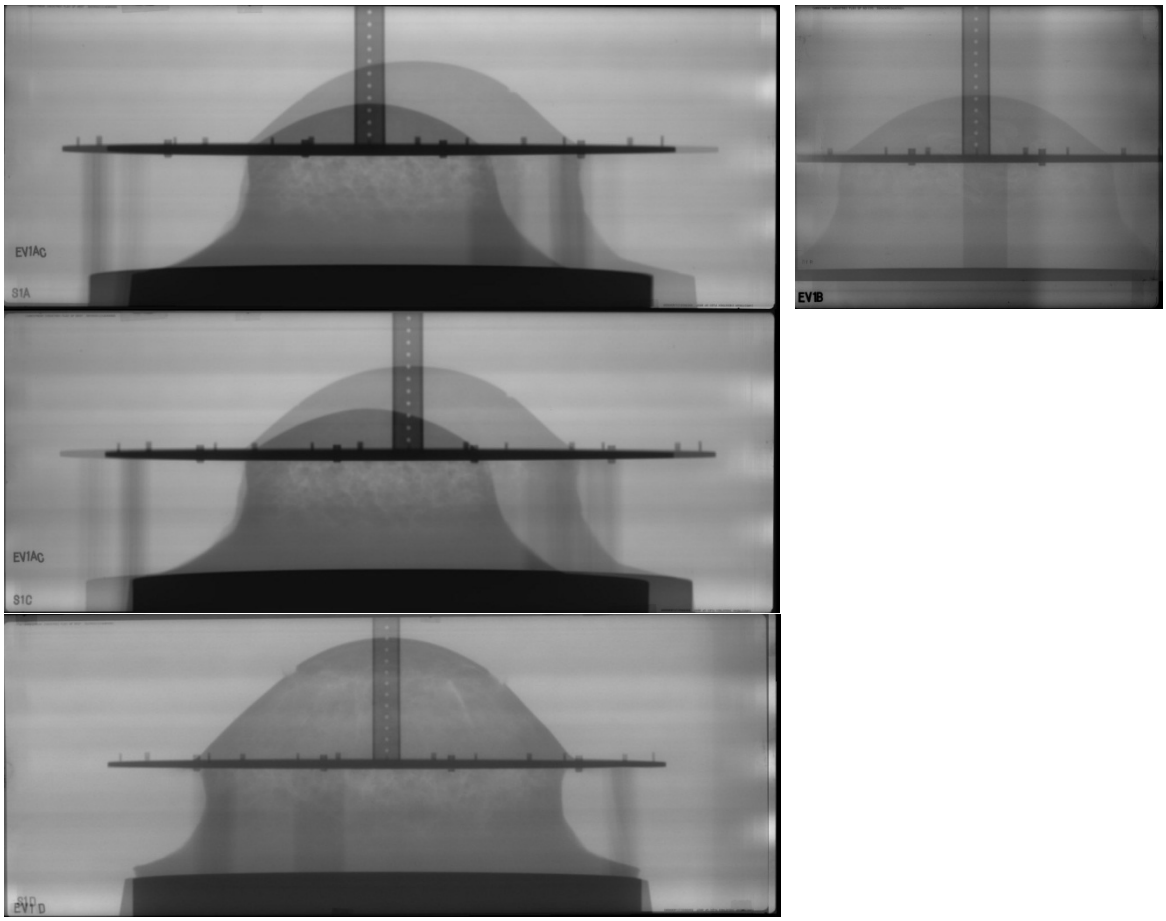

Event B2 – Silica sand, dry, ρ=1.57 g/cm³

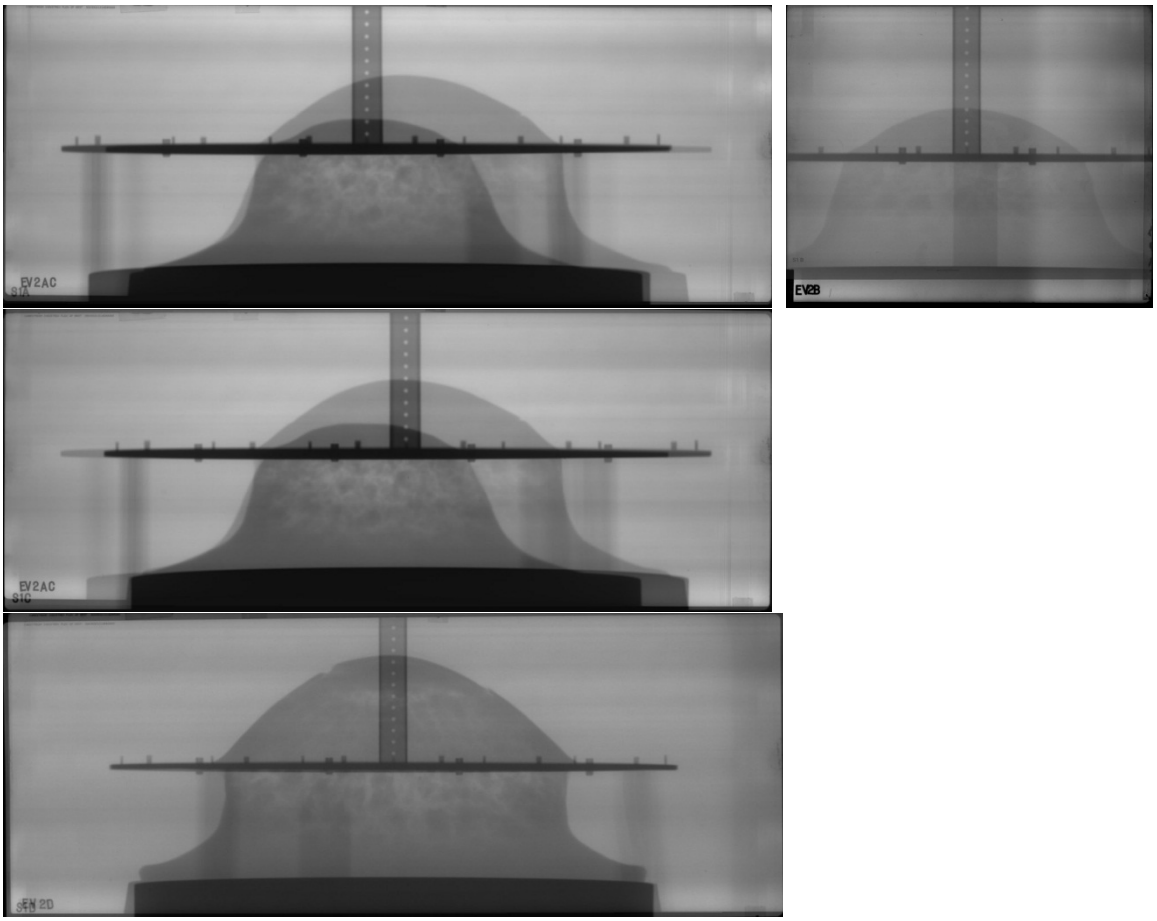

Event B3 – Coarse silica sand, dry, ρ=1.44 g/cm³

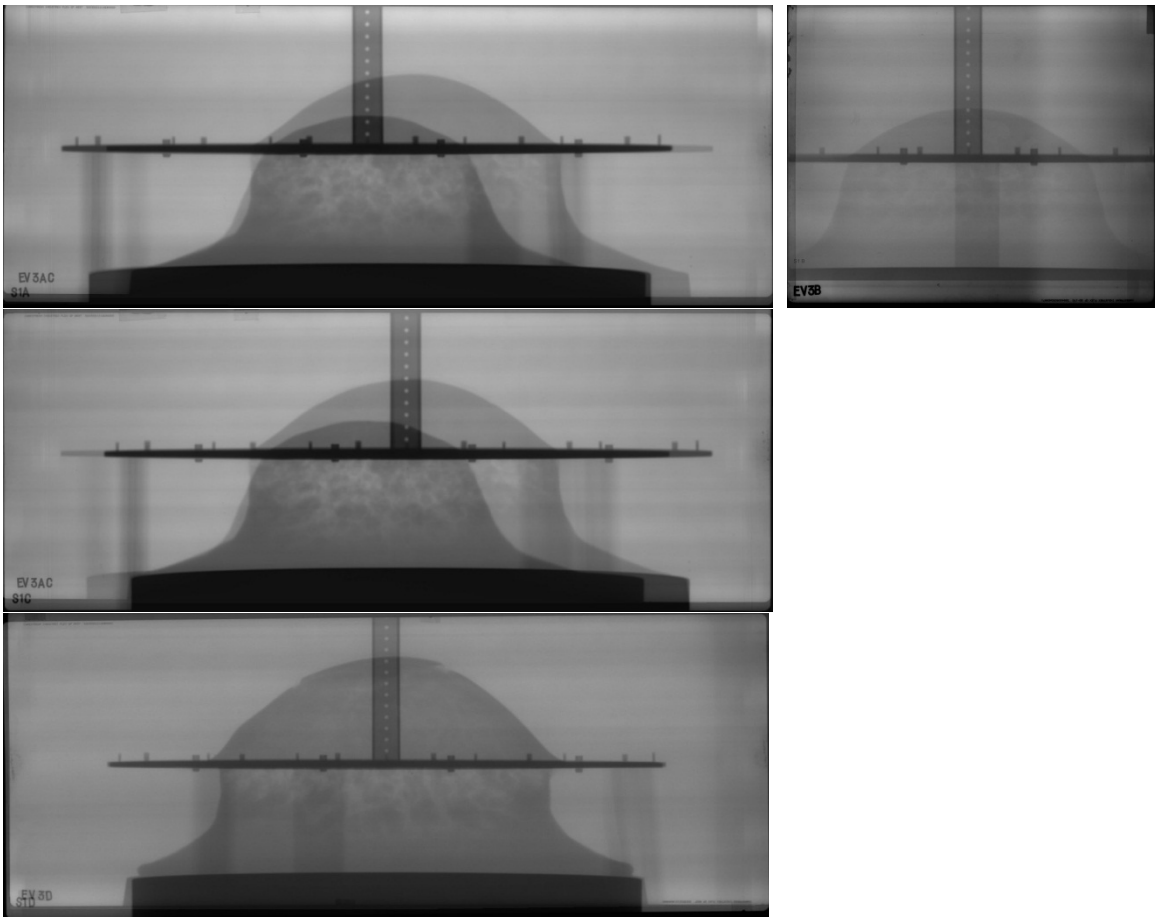

Event B4 – Calcium carbonate sand, dry, compacted, ρ=1.45 g/cm³

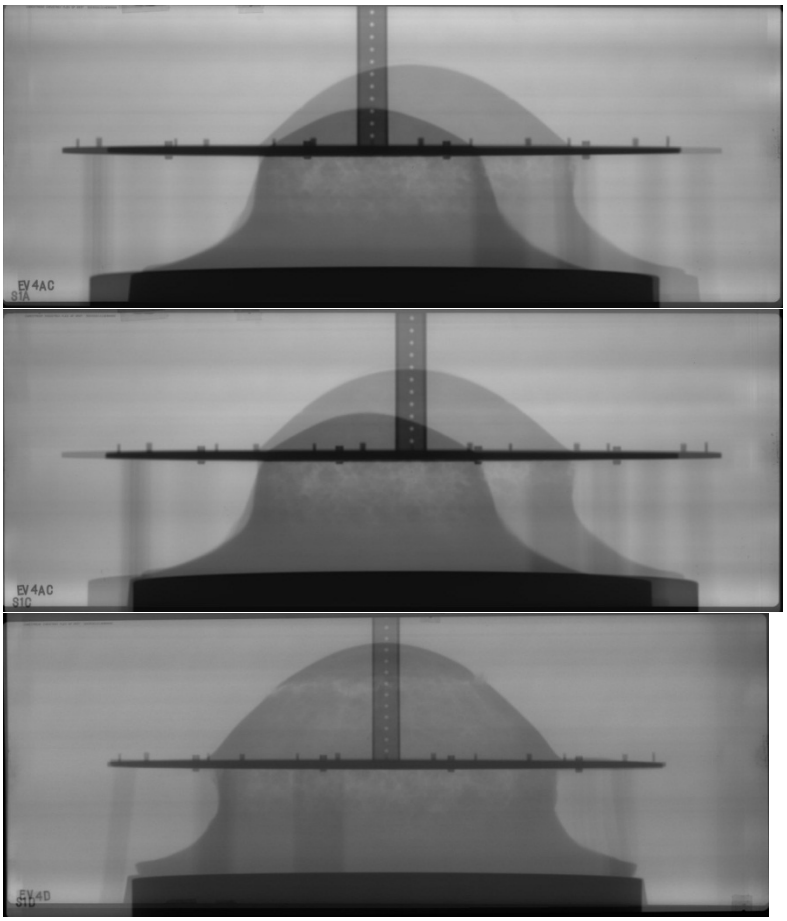

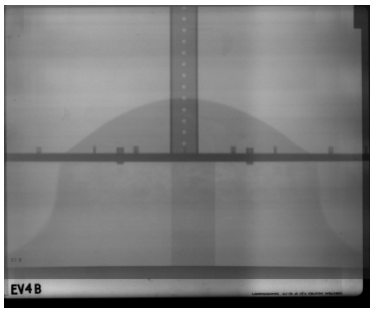

Event B5 – Glass beads, dry, ρ=1.48 g/cm³

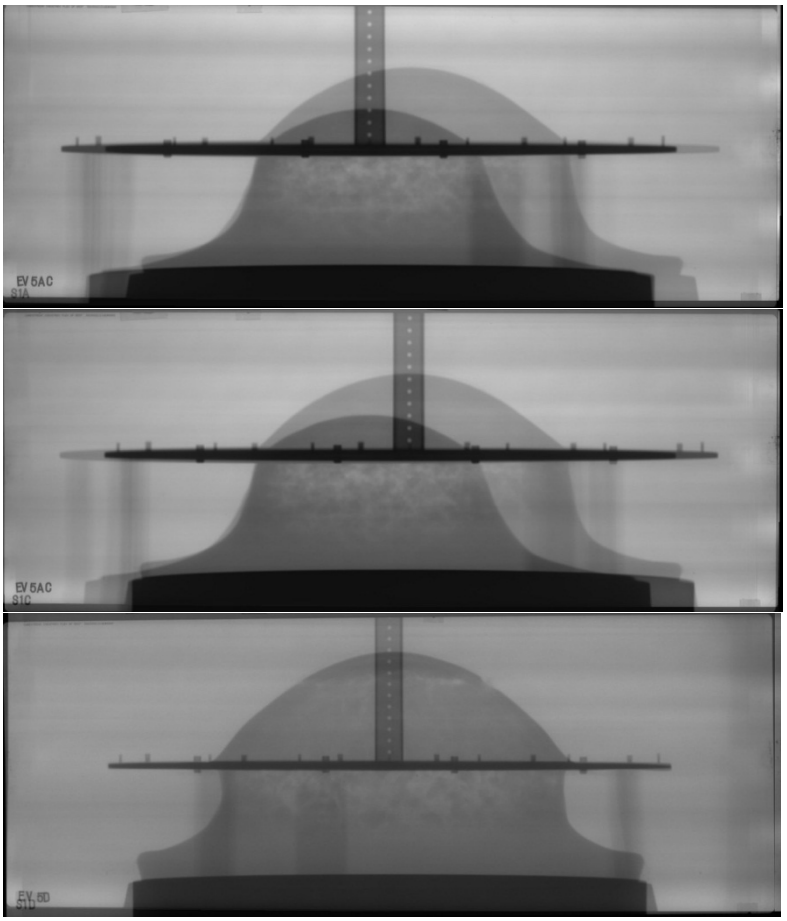

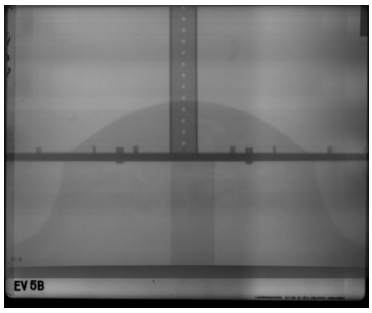

Event B6 – Diatomaceous earth, dry, ρ=0.14 g/cm³

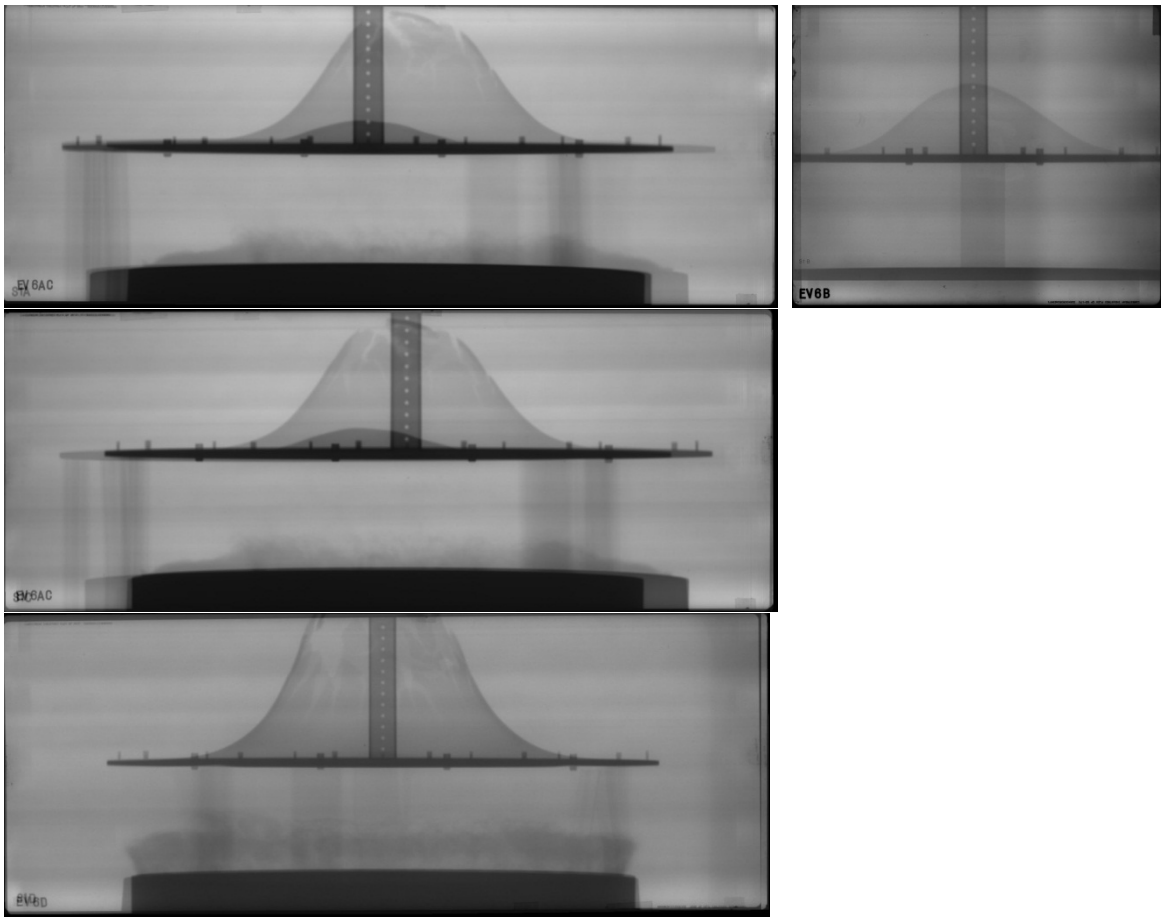

Event B7 – Coarse silica sand, 10% moisture, ρ=1.41 g/cm³

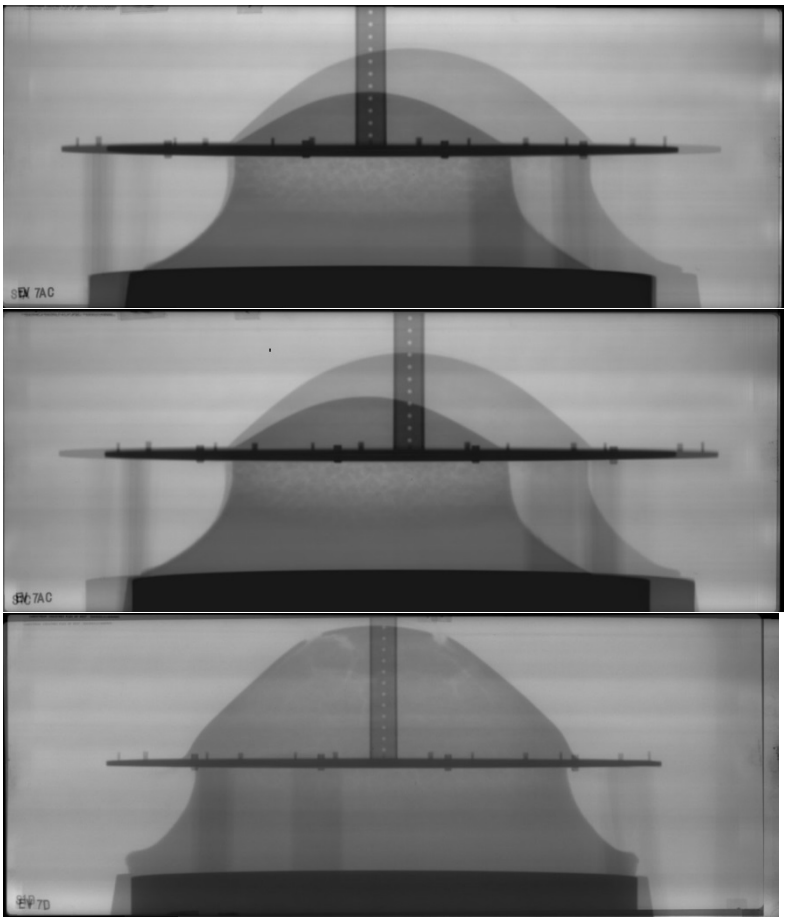

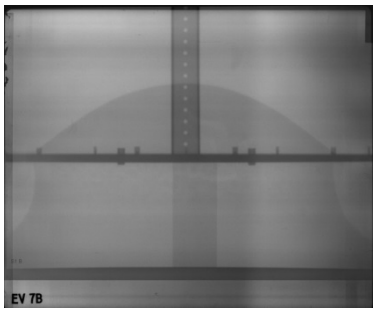

Event B8 – Silica sand, 10% moisture, ρ=1.58 g/cm³

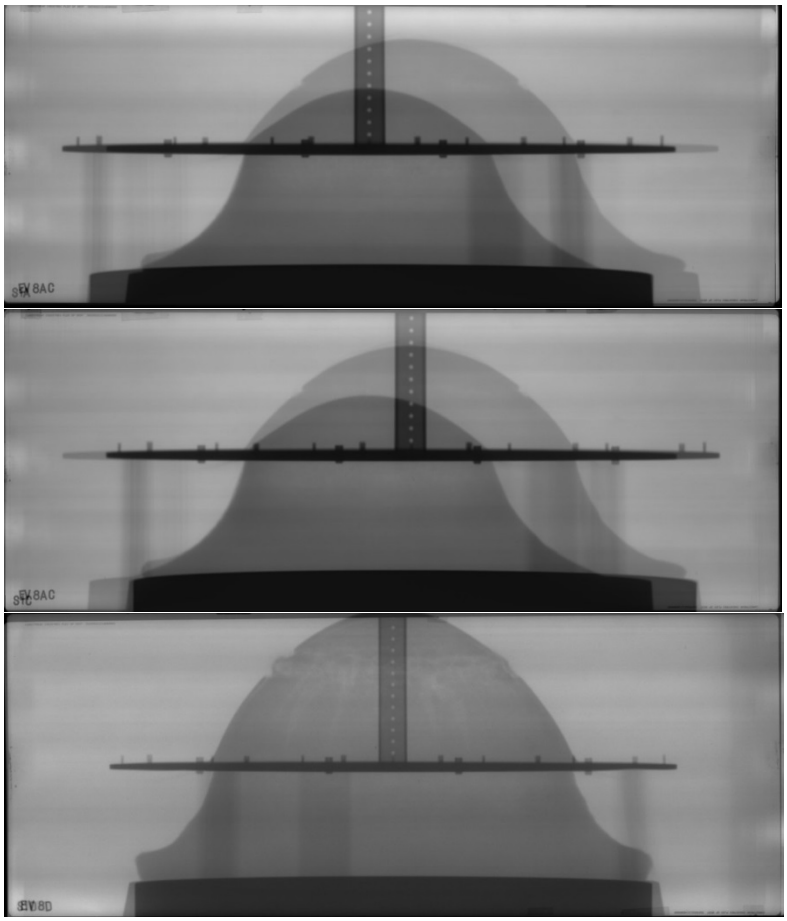

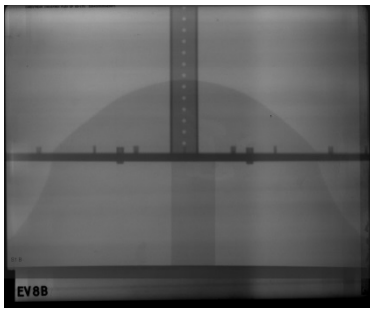

Event B9 – Calcium carbonate sand, 10% moisture, ρ=1.21 g/cm³

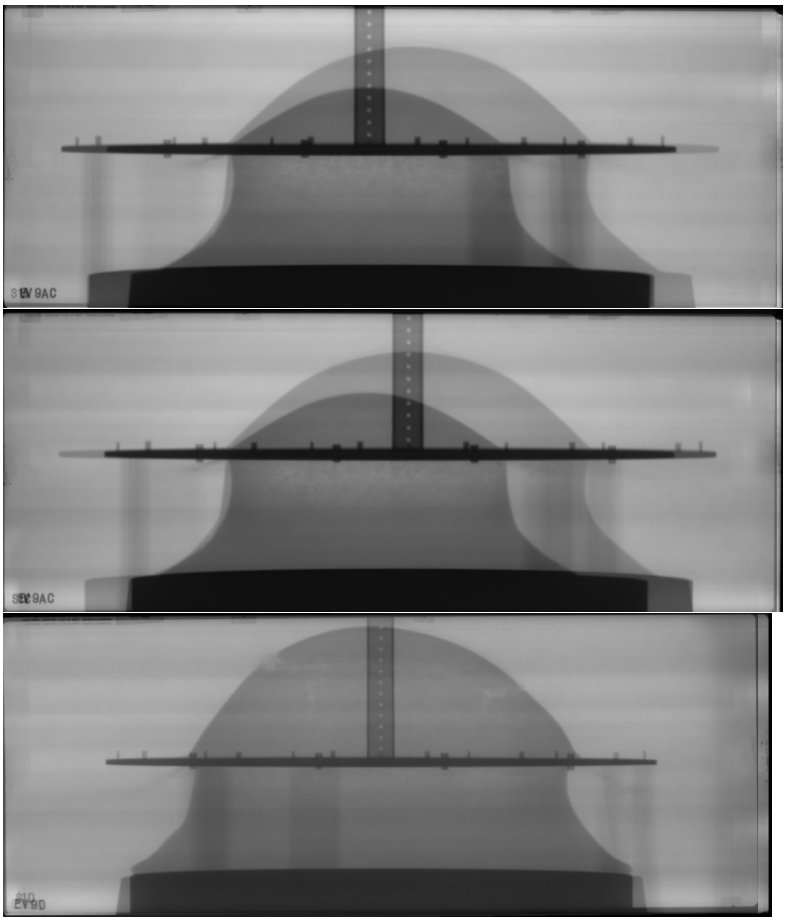

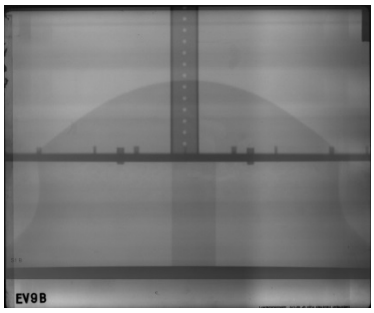

Event B10 – Road base, 7.0% moisture, ρ=2.05 g/cm³

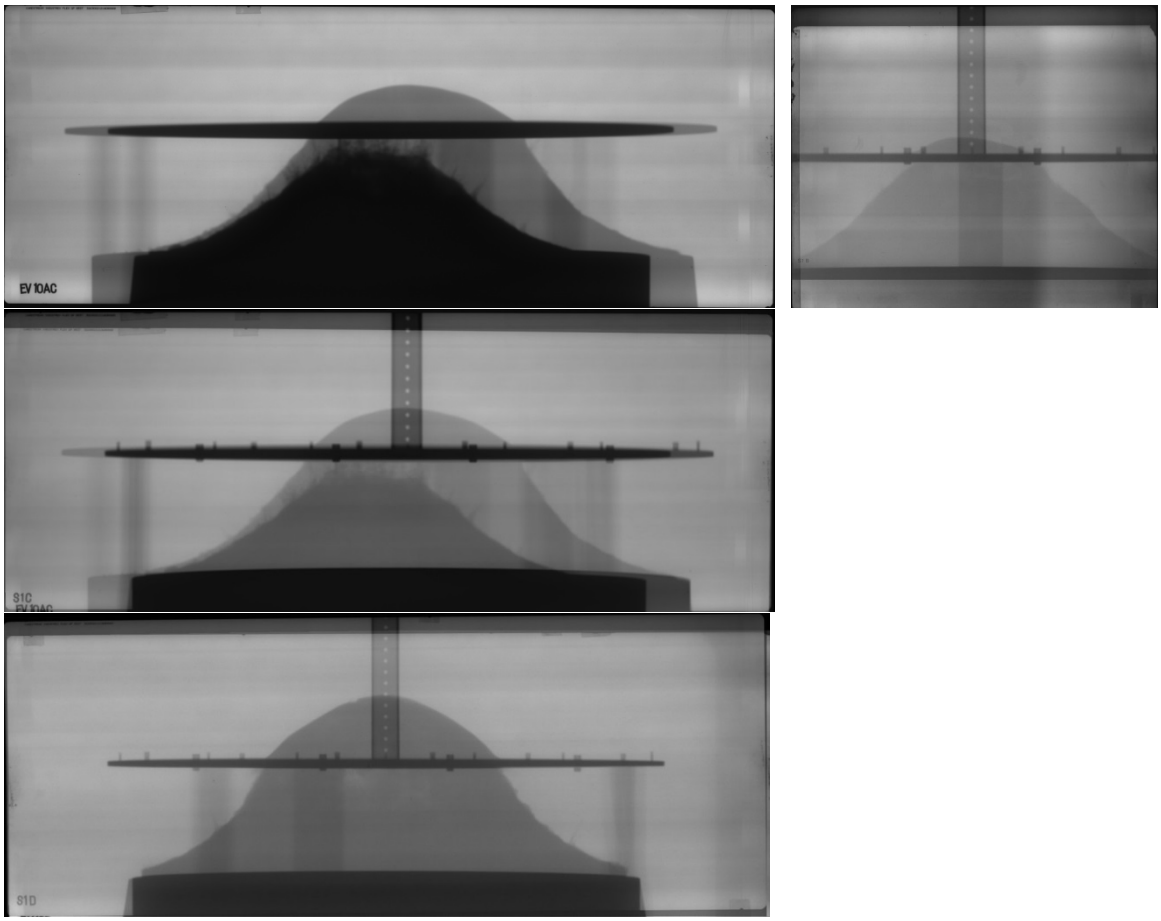

DEFENCE SCIENCE AND TECHNOLOGY GROUP DOCUMENT CONTROL DATA	1. DLM/CAVEAT (OF DOCUMENT)

2. TITLE	3. SECURITY CLASSIFICATION
Target Plate Deformation Time-History from a Detonating Buried Charge in Various Sand Media	Document (U) Title (U) Abstract (U)
4. AUTHOR(S)	5. CORPORATE AUTHOR
S. A. Weckert and A. D. Resnyansky	DST Group Edinburgh PO Box 1500 Edinburgh SA 5111

6a. DST Group NUMBER	6b. AR NUMBER	6c. TYPE OF REPORT	7. DOCUMENT DATE
DST-Group-TR-3609		Technical Report	June 2019

8. TASK NUMBER	10. TASK SPONSOR	11. RESEARCH DIVISION
	VCDF	Weapons and Combat Systems Division

12. MSTC	13. STC
Advanced Propulsion and Weapon Effects	Advanced Warhead Technologies

15. SECONDARY RELEASE STATEMENT OF THIS DOCUMENT

Approved for public release

OVERSEAS ENQUIRIES OUTSIDE STATED LIMITATIONS SHOULD BE REFERRED THROUGH DOCUMENT EXCHANGE, PO BOX 1500, EDINBURGH, SA 5111

16. DELIBERATE ANNOUNCEMENT

No limitations

17. CITATION IN OTHER DOCUMENTS Yes

18. RESEARCH LIBRARY THESAURUS

Flash X-ray; Buried charge; Porous material; Sand; Model validation

19. ABSTRACT

The present work analysed the influence of the sand/soil media for deforming a target plate in response to loading from a buried explosive charge. Flash x-ray technique was used to capture the plate deformation as a measure of the momentum transfer to the target. The target response was assessed experimentally for a variety of sands and a soil to investigate the effect of the sand parameters. The experiments used an axisymmetric cylindrical setup to enable easier comparison with numerical simulations in two-dimensions. The experiments were used to validate a two-phase model for the sand which has been implemented in the CTH hydrocode. Simulation results are in good agreement with the experiments and demonstrate a high fidelity description of the sand behaviour with the two-phase model.